To the Graduate Council:

I am submitting herewith a thesis written by Warren T. King entitled "Directional Solidification of Quaternary Eutectics." I recommend that it be accepted in partial fulfillment of the requirements for the degree of Master of Science, with a major in Metallurgical Engineering.

Ben F. Oliver, Major Professor

We have read this thesis
and recommend its acceptance:

C R Brooks

E. E. Stansbury

Accepted for the Council:

Vice Chancellor
Graduate Studies and Research

Thesis
78
K457
Cop. 2

DIRECTIONAL SOLIDIFICATION OF QUATERNARY EUTECTICS

A Thesis

Presented for the

Master of Science

Degree

The University of Tennessee, Knoxville

Warren T. King

June 1978

1358367

ACKNOWLEDGEMENTS

The author would like to express a most heartfelt gratitude and appreciation to Dr. B. F. Oliver who initiated and guided this research program, and who obtained the author's appointment as a Research Assistant at The University of Tennessee. Dr. Oliver advised and guided the author's educational and research efforts throughout his undergraduate and graduate studies and provided an excellent blend of theoretical and practical experience to the author.

The author would also like to thank Mr. B. L. McGill for his patient and thorough instruction and guidance in the operation of the scanning electron microscope.

Mr. T. A. Long, Mr. A. J. Beal and Mr. R. L. Johnson of the departmental electronic shop kept the electronic instrumentation necessary for this study in perfect working condition (especially the World War II vintage vacuum tube instruments) and provided a host of invaluable tips and suggestions. For this the author is extremely grateful.

The author would like to express his thanks to Mr. H. B. Thompson, Mr. Robert Love, Mr. J. G. French and Mr. Raymond Bellamy of the departmental machine shop for helping him rebuild the furnace unit the several times that it required and for their extremely helpful hints and suggestions.

Last, and most certainly not least, the author would like to thank his parents for their continuing support of his education, and without whom all this would not be possible.

ABSTRACT

The interest in obtaining materials with a novel set of properties has been a major factor in the large amount of work done on directional solidification in the past twenty years. The periodic structures obtained from directionally solidified eutectics show considerable potential for useful applications.

A substantial amount of theoretical and experimental work has been performed on binary eutectics. The theories developed describe the steady state transformation behavior of a class of binary eutectics moderately well.

The theoretical aspects of ternary systems are just now being examined. Experimental work has shown that some concepts of coupled two phase growth from the liquid can be extended to characterize the steady state coupled growth of three solid phases.

The Pb-Sn-Cd-Zn and the In-Sn-Cd-Zn quaternary systems were used as model systems to investigate the behavior of four phase eutectics. It was found that some of the concepts for coupled two and three phase eutectics can be extended to describe the quaternary eutectics.

TABLE OF CONTENTS

CHAPTER		PAGE
I.	INTRODUCTION AND THEORETICAL BACKGROUND	1
II.	APPARATUS AND EXPERIMENTAL PROCEDURE	12
III.	RESULTS AND DISCUSSION	17
	Selection of Quaternary System	17
	Temperature Profile at the Interface	19
	Observed Microstructures	24
	Pb-Sn-Cd-Zn	24
	In-Sn-Cd	24
	In-Sn-Cd-Zn	24
	Region of Coupled Growth	28
	Pb-Sn-Cd-Zn	28
	In-Sn-Cd-Zn	29
	Extremum Condition	30
	Pb-Sn-Cd-Zn	30
	In-Sn-Cd-Zn	32
	Dendrite Structures	35
	Types of dendrites	35
	Pb-Sn-Cd-Zn	35
	In-Sn-Cd	42
	In-Sn-Cd-Zn	42
	Spatial relationships of multiphase dendrites	42
	Pb-Sn-Cd-Zn	42
	In-Sn-Cd	50

CHAPTER PAGE

III. (Continued)

In-Sn-Cd-Zn 50

Path of solidification. 50

Composition effects 51

G/R effects 62

Velocity effects. 66

IV. CONCLUSIONS 72

LIST OF REFERENCES. 75

APPENDIX. 78

VITA. 88

LIST OF TABLES

TABLE		PAGE
I.	Interfacial Energies.	6
II.	Eutectic Compositions and Temperatures.	18
III.	Extension of Dendrites ahead of the Eutectic Interface. . .	52
IV.	Pb-Sn-Cd-Zn Experimental Results.	80
V.	In-Sn-Cd-Zn Experimental Results.	84

LIST OF FIGURES

FIGURE		PAGE
1.	Schematic solid-liquid interface of a binary eutectic. . . .	4
2.	High temperature gradient furnace.	13
3.	Schematic diagram of furnace	14
4.	Phase constitution diagrams in the Pb-Sn-Cd-Zn system. . . .	20
5.	Phase constitution diagrams in the In-Sn-Cd-Zn system. . . .	21
6.	Strip chart recorder trace of temperature profile of Ingot 1076.	22
7.	Coupled Pb-Sn-Cd-Zn eutectic	25
8.	Coupled In-Sn-Cd eutectic.	26
9.	Coupled In-Sn-Cd-Zn eutectic	27
10.	The variation of the lamellar spacing with velocity in the Pb-Sn-Cd-Zn system.	31
11.	Lamellar spacing of the high and low gradient Pb-Sn-Cd-Zn alloys	33
12.	The variation of the lamellar spacing with velocity in the In-Sn-Cd-Zn system.	34
13.	Dendrites in the Pb-Sn-Cd-Zn quaternary.	36
14.	Dendrites in the In-Sn-Cd ternary.	43
15.	Dendrites in the In-Sn-Cd-Zn quaternary.	46
16.	Typical microstructure of Ingot 1080	54
17.	Schematic solid-liquid interface of Ingot 1080	55
18.	Typical microstructure of Ingot 1102	56
19.	Typical microstructure of Ingot 1098	58

FIGURE PAGE

20. Typical microstructure of Ingot 1096 59

21. Typical microstructure of Ingot 1074 60

22. Effect of growth conditions on the steady state solidification path. 63

23. Variation in dendrite structure with growth conditions in Ingot 1102. 67

24. Effect of growth velocity on the Cd-Sn dendrites in Ingot 1076. 70

CHAPTER I

INTRODUCTION AND THEORETICAL BACKGROUND

Directional solidification had its start in 1952 when W. G. Pfann[1] demonstrated that zone refining was a feasible method to produce germanium both pure and structurally sound enough to exhibit semiconducting properties.

Rutter and Chalmers[2] coupled the mass transfer problem studied by Pfann with the thermal gradient in the liquid in front of the solififying interface to define a thermodynamic instability in the liquid called "constitutional supercooling."

When the solid-liquid interface moves at a steady state, non-zero velocity, a composition boundary layer exists in the liquid which can be described by the phase constitution of the system and the rate of diffusion of the species in the liquid. By referring to the phase diagram, an equilibrium solidification temperature can be specified for each composition in the boundary layer. Given the appropriate conditions of growth velocity and thermal gradient in the liquid, some regions of the boundary layer can be below its corresponding equilibrium solidification temperature and therefore be supercooled. The undercooled region is the constitutionally supercooled liquid.

Tiller, Jackson, Chalmers and Rutter[3] addressed the problem of a single phase, two component system quantitatively and developed the following stability criterion where constitutional supercooling

can be avoided:

$$\frac{G}{R} \geq \frac{mC_o(1-k)}{Dk} \quad , \qquad (1)$$

where: G = thermal gradient in the liquid in front of the solid-liquid interface,

R = interface growth velocity,

m = slope of the liquidus,

C_o = initial (bulk) composition of the alloy,

D = diffusion coefficient of the solute in the liquid, and

k = distribution coefficient, the ratio of the equilibrium compositions of the solid to that of the liquid at the interface.

Mullins and Sekerka[4] later developed a stability criterion for single phase growth by examining the stability of a perturbation in the solid-liquid interface. They showed that the stability of the interface depended on three quantities. The first quantity was the solid-liquid interfacial energy, which was found to stabilize the interface. The second was a thermal gradient term which, under the conditions necessary for directional solidification, also stabilized the interface. The last quantity was a phase constitution term which could be directly related to Equation 1.

Tiller[5] examined the mass transfer problem for the growth of two solid phases from the liquid for the eutectic reaction:

$$L \rightarrow S_1 + S_2 \quad .$$

The steady state growth of regular, lamellar eutectics was of interest. Tiller developed an existence condition for the coupled structure. The solid-liquid interface was assumed to be the one shown in Figure 1. For the system shown, the free energy required to form the α-β interface can only be supplied by the free energy change of the liquid to solid transformation.

If the liquid solidifies reversibly at the eutectic temperature, there is no free energy change. Some undercooling is therefore necessary to supply the free energy of formation of the α-β interfaces. This undercooling can be calculated if the heat of fusion of the eutectic, the α-β interfacial energy and the lamellar spacing are known. The calculated undercooling is the bulk or average undercooling of the liquid that is required to supply the free energy for the interfaces.

The solid phases are assumed to have curved surfaces at the solid-liquid interface (see Figure 1). The Gibbs-Thomson potential, which relates a change in the equilibrium melting point with the curvature of the interface, can be used to calculate the temperatures below the eutectic temperature at which both phases will solidify. If the average undercooling of the liquid required to form the solid-solid interfaces is assumed to be equal to the weighted average of the undercoolings of the individual phases due to curvature, then the following inequality results:

$$\frac{\sigma_{\alpha\beta}}{\Delta S} < \frac{\sigma_{\alpha L}}{\Delta S_{\alpha}} + \frac{\sigma_{\beta L}}{\Delta S_{\beta}} \quad , \qquad (2)$$

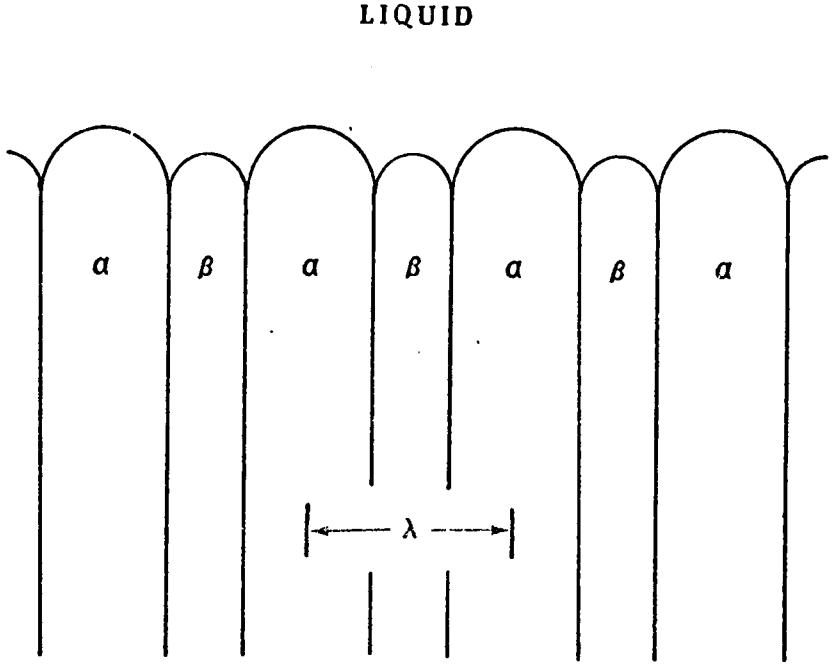


Figure 1. Schematic solid-liquid interface of a binary eutectic.

where: $\sigma_{\alpha\beta}$ = α-β solid interfacial energy,

$\sigma_{\alpha L}$ = α-liquid interfacial energy,

$\sigma_{\beta L}$ = β-liquid interfacial energy,

ΔS = entropy of fusion per unit volume of the eutectic,

ΔS_{α} = entropy of fusion per unit volume of α, and

ΔS_{β} = entropy of fusion per unit volume of β.

This existence condition can be extended to lamellar eutectics of more than two phases by accounting for the additional interfaces that are present due to the additional phases present during solidification.

The existence condition is a statement of the necessary energy balance that must be satisfied in order for a regular, steady state structure to exist. The condition does not predict which structure will be experimentally obtained. For example, the Pb-Sn-Cd ternary eutectic is known to have a regular Sn-Pb-Cd-Pb-Sn arrangement[6,7]. Assuming that the structure is perfectly periodic and regular, the existence condition is given by:

$$\frac{\sigma_{Pb\text{-}Sn} + \sigma_{Pb\text{-}Cd}}{\Delta S} < \frac{\sigma_{Cd\text{-}L}}{\Delta S_{Cd}} + \frac{\sigma_{Sn\text{-}L}}{\Delta S_{Sn}} + \frac{2\sigma_{Pb\text{-}L}}{\Delta S_{Pb}} , \qquad (3)$$

The interfacial energies are given in Table I. From Kubackewski, Evans and Alcock[8], the entropies of fusion of Pb, Sn and Cd at the eutectic temperature, 145°C, are 0.0935, 0.207 and 0.190 cal/cm^{3}K, respectively. The weighted entropy of fusion of the eutec-

TABLE I

INTERFACIAL ENERGIES

Interface	Interfacial Energy (erg/cm^2)
Pb-liquid[a]	33.3[9], 69[10]
Sn-liquid[a]	59[9]
Cd-liquid[b]	57.6[11]
Bi-liquid[a]	54.4[9]
Zn-liquid[a]	121[12]
In-liquid	not available
Pb-Sn	35[13], 47[14], 42[15]
Pb-Cd	11[13], 13[14]
Sn-Cd	75[16]
Sn-Zn	115[17], 77[17], 120[17]
Cd-Zn	86[18], 54[18]
Pb-Zn	not available
Bi-Pb_2Bi	134[19]
Bi-Cd	110[19]
Bi-Sn	not available
Bi-Zn	32[18], 70[18]
In-Sn	not available
In-Cd	not available
In-Zn	not available

[a]Based on undercooling experiments.

[b]Calculated value.

tic is 0.177 cal/cm^{3}K. The existence condition is numerically satisfied when these values are used.

If the arrangement Pb-Sn-Cd-Pb-Sn-Cd were considered, the resulting existence condition would be:

$$\frac{\sigma_{Pb\text{-}Sn} + \sigma_{Pb\text{-}Cd} + \sigma_{Sn\text{-}Cd}}{\Delta S} < \frac{\sigma_{Cd\text{-}L}}{\Delta S_{Cd}} + \frac{\sigma_{Sn\text{-}L}}{\Delta S_{Sn}} + \frac{\sigma_{Pb\text{-}L}}{\Delta S_{Pb}} \quad . \quad (4)$$

Equation 4 is also numerically satisfied. The solid-solid interfacial energies are sufficiently small that any arrangement of the three phases in a regular structure would satisfy its corresponding existence condition.

The reason for the experimentally observed structure apparently lies in the relative values of the solid-solid interfacial energies. The Sn-Cd interfacial energy is large compared to the Pb-Sn and the Pb-Cd interfacial energies. The resultant structure was one where the highest energy interface was absent.

To check the validity of the existence condition, the Bi-Cd eutectic, which is an anomalous eutectic, was used. The entropies of fusion of Bi and Cd at the eutectic temperature, 145.5°C, are 0.244 and 0.190 cal/cm^{3}K, respectively. The weighted entropy of fusion of the eutectic is 0.209 cal/cm^{3}K. The existence condition (Equation 2) is not satisfied when these values are used. This agrees with the non-lamellar structure of the eutectic. The inequality is not satisfied because of the high Bi-Cd solid interfacial energy as compared to the solid interfacial energies in the Pb-Sn-Cd system.

Tiller also examined the problem of the width of binary, lamellar eutectics based on the constraints imposed by the rate of diffusion of the species in the liquid and the formation of the solid α-β interfaces.

The interface shown in Figure 1 was considered. As the interface moves forward, A atoms are rejected in front of the β phase and diffuse towards the α phase while B atoms are rejected in front of the α phase and diffuse towards the β phase. For a given lamellar spacing, the interface cannot move faster than the A and B atoms can diffuse to the α and β phases if a steady state process is maintained. Conversely, if the interface growth velocity is fixed, the width of the phases is limited by the rate of diffusion of the A and B atoms.

Tiller assumed that the eutectic would grow in a manner that would minimize the total energy of the system. Since the formation of the solid interfaces costs energy, the total amount of interface per unit volume of the eutectic would be minimized. Smaller lamellar widths increases the total amount of interface present. The effect of the interfacial energy would be to increase the lamellar width.

Using an approximate mass and energy balance at the interface, Tiller suggested a relationship between the average undercooling of the interface, ΔT, the growth velocity, R, and the lamellar width, λ. Hunt and Jackson[20] later followed Tiller's analysis in a more mathematically detailed fashion and found a similar relation between the three variables. The relation is:

$$\Delta T = K_1 \lambda R + K_2/\lambda \quad , \qquad (5)$$

where K_1 and K_2 are constants that depend on the equilibrium relationships of the phases and on material properties such as interfacial energies, diffusivities and heats of fusion.

Since we only have one equation to relate the three variables, this implies that any one of the three can be fixed while the other two can be varied independently as long as Equation 5 is satisfied. It is observed experimentally that a unique lamellar width corresponds to a given growth velocity. The theory is therefore incomplete and requires an additional assumption in order to explain the observed results.

The statement of the extremum conditions for coupled growth results when the assumption is made that the growth of the eutectic occurs at the maximum velocity or at the minimum undercooling (both assumptions being mathematically equivalent). The extremum conditions for coupled growth of a binary eutectic are:

$$\lambda^2 R = \text{constant} \quad , \qquad (6a)$$

$$\Delta T^2/R = \text{constant} \quad , \text{ and} \qquad (6b)$$

$$\Delta T\lambda = \text{constant} \quad . \qquad (6c)$$

These conditions have been found to be obeyed experimentally.

Bao and Durand[21] analyzed ternary eutectic growth in a manner following Hunt and Jackson's treatment and found the same extremum conditions for coupled growth of ternary eutectics. Work

done on the ternary Pb-Sn-Cd system[7,21] has shown that the extremum conditions are obeyed.

Cline[22] used Hunt and Jackson's results and considered the stability of the multiphase interface in a fashion similar to Mullins and Sekerka's analysis of single phase alloys. For stable coupled two phase growth, Cline showed that the following relation must be satisfied:

$$\frac{G}{R} \geq \frac{1}{2} \frac{(K_S + K_L)}{K_L} \frac{(C_0 - C_E)}{D} m^* \quad , \qquad (7)$$

where: K_S = solid thermal conductivity,

K_L = liquid thermal conductivity,

C_0 = initial (bulk) composition of the alloy,

C_E = eutectic composition,

D = diffusion coefficient of the species in the liquid, and

m^* = effective liquidus slope.

Experimentally, Equation 7 has been shown to accurately predict the region of coupled growth in binary eutectics.

Rinaldi, Sharp and Flemings[23] developed a theoretical statement for the coupled growth of three phase eutectics based on a simple constitutional supercooling model similar to the one developed for single phase alloys (Equation 1). Work on the ternary Pb-Sn-Cd system[7] has shown that their model does not adequately predict the regions of coupled growth encountered in the ternary system.

Little experimental and theoretical work has been performed on quaternary systems. Recently, Fisher and Kurz[24] examined the microstructures of directionally solidified Pb-Sn-Cd-Zn eutectic alloys. They found that coupled four phase structures were possible. All four phases were lamellar, with the Pb, Sn and Cd phases retaining the ternary Sn-Pb-Cd-Pb-Sn arrangement and the Zn phase perpendicular to the other three phases and contained mainly within the Sn phase. The eutectic obeyed the $\lambda^2 R$ extremum condition. The lamellar spacing of the quaternary is similar to that of the ternary Pb-Sn-Cd reported by Bao and Durand[21].

CHAPTER II

APPARATUS AND EXPERIMENTAL PROCEDURE

The high temperature gradient furnace used by Holder and Oliver[7] was used in this study (Figure 2). The furnace was designed to produce a flat solid-liquid interface with a high temperature gradient in the liquid in front of the interface. The furnace consists of (see schematic of furnace in Figure 3):

1 resistance heating element,

2 water heat sink (water temperature controlled by a refrigerator),

3 silver heat sleeve,

4 mica washer, and

5 shielded control thermocouple.

Temperature gradients of up to 400 °C/cm could be obtained. The drive mechanism could provide growth rates from 0.35×10^{-4} to 40×10^{-4} cm/sec. Unfortunately, velocity perturbations were observed in specimens grown at less than 1×10^{-4} cm/sec. The problem could not be eliminated and useful data exists only for velocities above this value.

The ingots were made by drawing molten alloy of desired composition into a 4 mm OD, thin walled silica tube. A chromel-alumel thermocouple, made of 7.6 μm wires insulated with MgO and sheathed in 316 stainless steel (0.52 mm OD), was inserted into the bottom of the ingot.

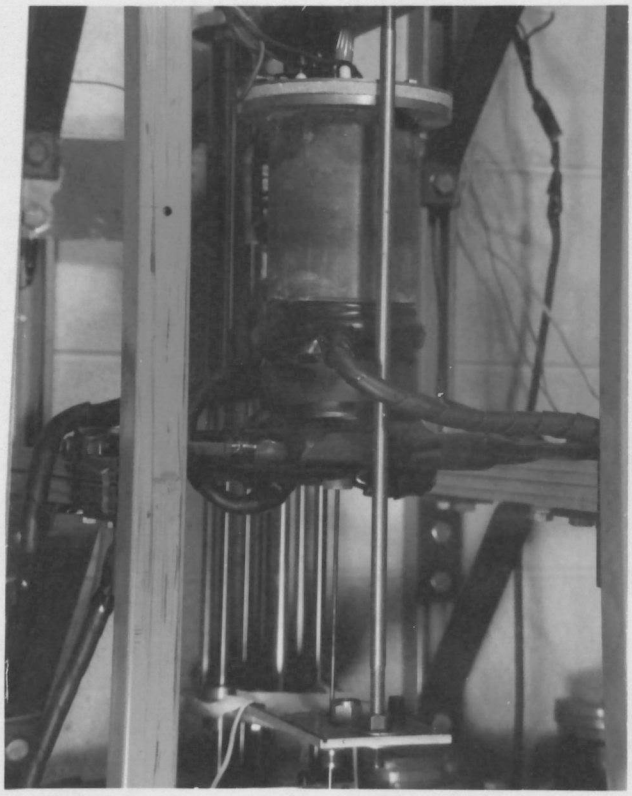


Figure 2. High temperature gradient furnace.

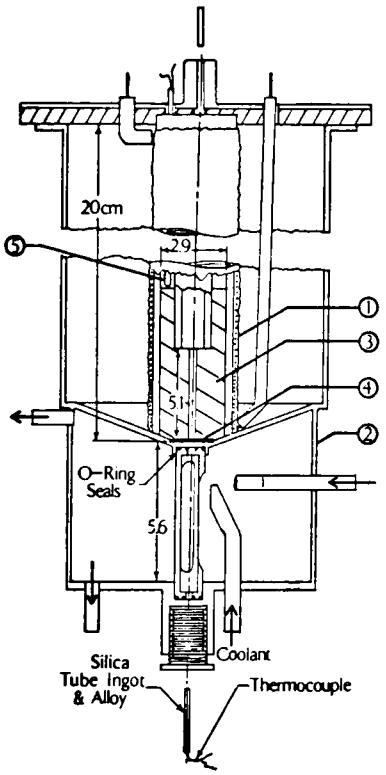


Figure 3. Schematic diagram of furnace.

When the furnace was at the proper temperature, the ingot was inserted into the bottom of the furnace and back melted until the thermocouple tip was surrounded by liquid. The drive mechanism was started and the thermocouple was used to measure the temperature gradient in the ingot. To facilitate data taking, 7 to 10 specimens directionally solidified at different velocities could be obtained from each ingot. The different velocities were run in random order so that changes in the microstructures due to changes in growth conditions can be distinguished from those due to segregation in the ingots.

The microstructures were determined by metallographic examination. Transverse and longidudinal sections of each specimen were prepared for optical and SEM micrography. The longitudinal sections were useful in ensuring that the solid-liquid interface was flat and that that specimen was uniform in structure throughout its length without perturbations.

An electrolytic etch of 0.25% Br in methanol mixed 20:1 with water for 3 seconds at room temperature, 4.5 V and 0.35 amps/cm^2 was found to work best for the Pb-Sn-Cd-Zn alloys. The In-Sn-Cd-Zn alloys were etched electrolytically in a solution of 5% perchloric acid in methanol for 1 second at 0°C, 30 V and 6 amps/cm^2. The etchants left a residue on the surface of the specimens that was easily removed by using an ultrasonic cleaner.

The lamellar spacings of the specimens were measured using the optical microscope. The magnification was calibrated each time measurements were made by using a stage micrometer. The spacings

were measured in a minimum of five different grains in each specimen. The measurements were made across 5 to 10 uninterrupted lamellae to obtain an average value.

CHAPTER III

RESULTS AND DISCUSSION

I. SELECTION OF QUATERNARY SYSTEM

An important factor in the choice of the systems to be studied was the availability of phase constitution data. At a minimum, the eutectic temperature and composition should be known. There should preferably not be complicating solid state reactions to obscure the solidification microstructure. Six quaternary systems of interest were found for preliminary study. Their eutectic compositions and temperatures are listed in Table II.

Compatibility with the experimental setup was also considered. Bismuth and high bismuth alloys (>40%) expand after solidification. The silica tubes containing the eutectic alloys shattered after the metal was drawn. Directional solidification of the alloys in stainless steel tubes was attempted. Metallographic examination of the specimens after the experiment showed that the molten alloys heavily attacked the inner walls of the tube. Since a major modification of the experimental procedure and equipment was required for these alloys, they were dropped from further consideration.

Both of the remaining quaternary systems have a very small amount of Zn at the eutectic compositions. The Pb-Sn-Cd-Zn eutectic has about 2.6% Zn by volume while the In-Sn-Cd-Zn has about 0.8% Zn by volume at the eutectic composition.

TABLE II

EUTECTIC COMPOSITIONS AND TEMPERATURES

System	Eutectic Composition (wt. %) Pb	In	Bi	Sn	Cd	Zn	Eutectic Temperature (c)	Reference
Pb-Sn-Cd	32.0	----	----	50.0	18.0	----	145	(25)
In-Sn-Cd	----	44.0	----	42.0	14.0	----	93	(26)
Pb-Sn-Cd-Zn	28.60	----	----	52.45	16.70	2.25	138	(27)
Pb-Bi-Sn-Cd	27.27	----	49.50	13.13	10.10	----	70	(28)
Pb-Bi-Sn-Zn	30.00	----	53.20	16.25	----	0.75	93.5	(29)
Bi-Sn-Cd-Zn	----	----	54.50	25.25	19.25	1.00	100	(29)
Pb-Bi-Cd-Zn	39.0	----	52.8	----	8.0	0.2	91	(29)
In-Sn-Cd-Zn	----	44.2	----	41.4	13.6	0.8	90	(30)

The phase diagrams of the two quaternaries and their corresponding ternaries composed of the three major phases (by volume) are shown in Figures 4 and 5.

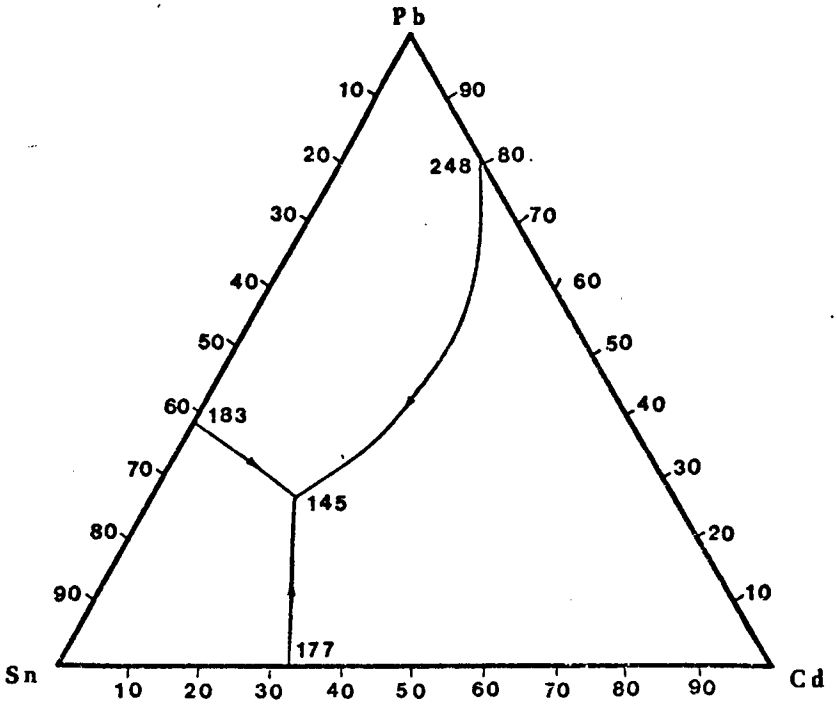
II. TEMPERATURE PROFILE AT THE INTERFACE

The thermocouple imbedded in the ingot was used to measure a) the temperature of the liquid as a function of the distance ahead of the interface, b) the temperature or temperature range of the liquid to solid transformation, and c) the temperature of the solid behind the interface. Figure 6 shows a typical thermocouple output traced by a strip chart recorder.

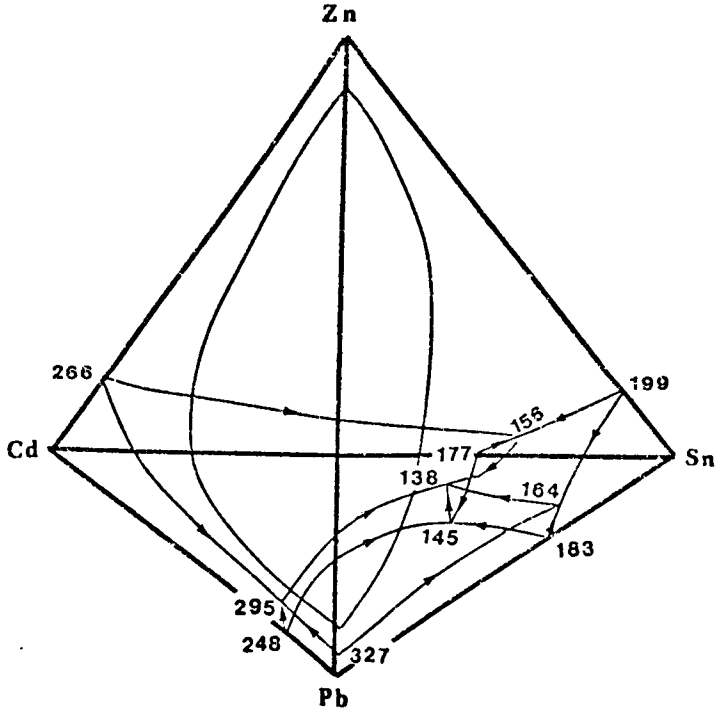
When coupled growth occured, a sharp break in the temperature profile was observed. In the Pb-Sn-Cd-Zn system, the breaks occured at 145 ± 1°C for the ternary Pb-Sn-Cd alloys and at 138 ± 1°C for the quaternary Pb-Sn-Cd-Zn alloys. Both temperature breaks occured at the eutectic temperatures. The temperature break for the In-Sn-Cd ternary alloys also occured at its eutectic temperature of 93°C.

Anomalous results were obtained for the In-Sn-Cd-Zn alloys. The thermal breaks were observed at 86°C instead of the published value of 90°C.

Non-directional furnace cooling experiments were performed on an alloy of eutectic composition to check these results. The thermal arrest of the eutectic was found to agree with the thermal breaks of the directionally solidified alloys to within 1°C. The

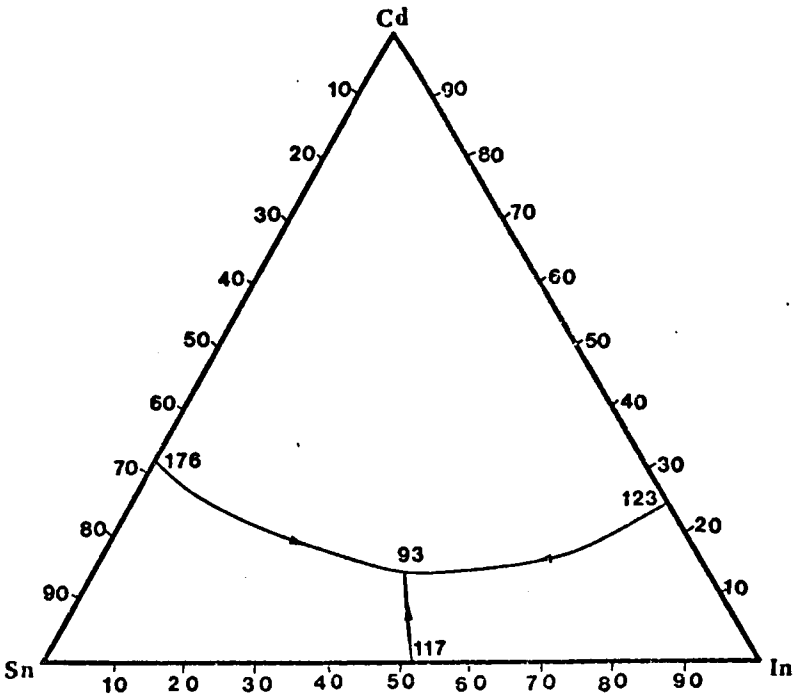


(a) Pb-Sn-Cd.

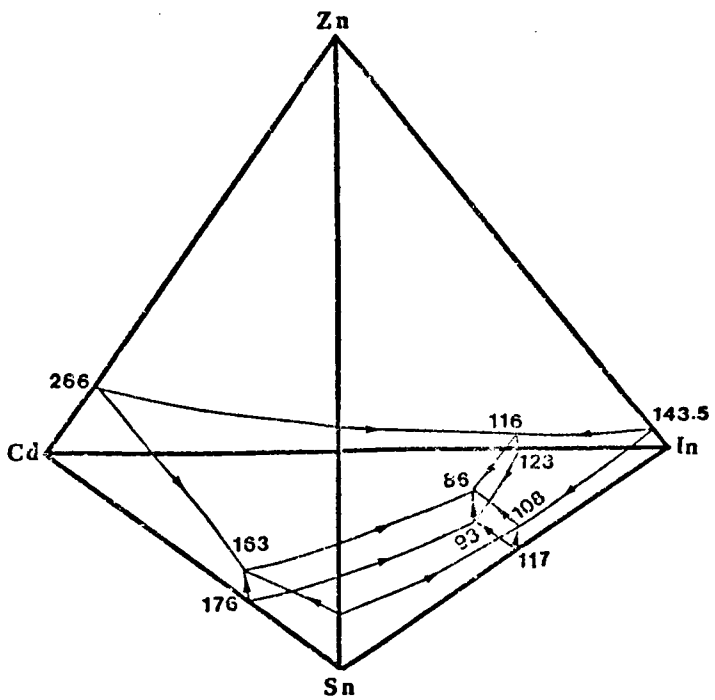


(b) Pb-Sn-Cd-Zn

Figure 4. Phase constitution diagrams in the Pb-Sn-Cd-Zn system.



(a) In-Sn-Cd.



(b) In-Sn-Cd-Zn.

Figure 5. Phase constitution diagrams in the In-Sn-Cd-Zn system.

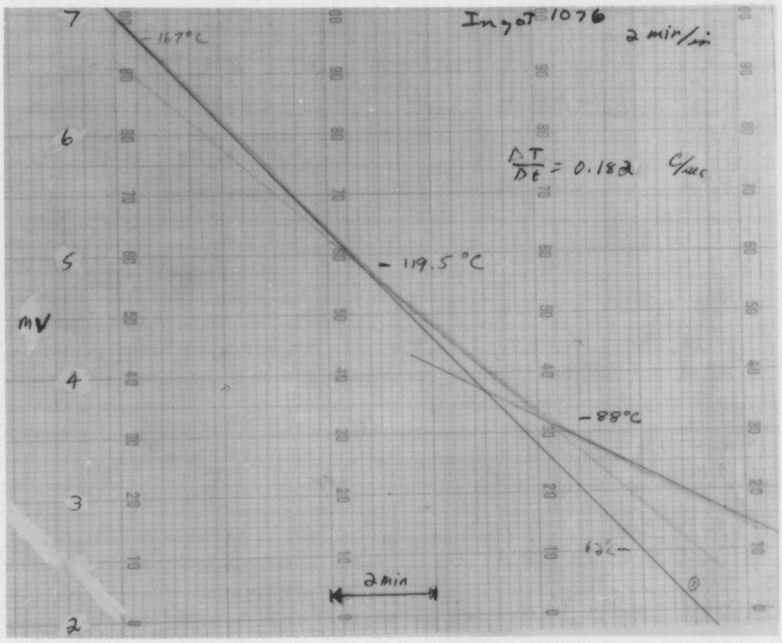


Figure 6. Strip chart recorder trace of temperature profile of Ingot 1076. R = 8.26 x 10^{-4} cm/sec.

thermocouples were checked by obtaining cooling curves for pure tin and indium. The thermocouples were found to be accurate to within 1°C.

Two thermal breaks above the eutectic temperature were observed in the cooling curves of the In-Sn-Cd-Zn eutectic alloy. Metallographic examination revealed the presence of Sn and Cd dendrites. This indicated that the published eutectic composition is also incorrect and that the true eutectic composition is richer in either In or Zn, or both.

When the solid-liquid interface was unstable and dendrites were observed, the temperature profile exhibited either 1) a rounded, instead of a sharp, thermal break, or 2) two thermal breaks.

When the thermal break was rounded, the extrapolated temperatures from the liquid and the solid intersected at the eutectic temperature.

The lower temperature of the two thermal breaks is the quaternary eutectic temperature. The higher temperature is within 5°C of the liquidus temperature of the ingot.

Lindner[27] published extensive liquidus information on the Pb-Sn-Cd-Zn system which was used to correlate the observed thermal breaks with the liquidus temperature. The liquidus of the In-Sn-Cd-Zn system is not available. The liquidus of the ternary In-Sn-Cd[26] was used as an approximation because of the small amount of Zn in the quaternary eutectic (about 0.8% Zn). The thermal breaks were within 5°C of the liquidus temperature of the ternary alloys of approximately the same composition as the quaternary alloys.

III. OBSERVED MICROSTRUCTURES

Pb-Sn-Cd-Zn

Fisher and Kurz[24] examined the microstructures of directionally solidified Pb-Sn-Cd-Zn eutectic alloys. They found that the lamellar Pb-Sn-Cd ternary eutectic structure was retained in the quaternary eutectic, with the Zn phase also lamellar and growing perpendicular to the other three phases. The Zn phase is almost entirely contained within the Sn phase. The results of this work are in agreement with the previous work. The observed four phase structure is shown in Figure 7.

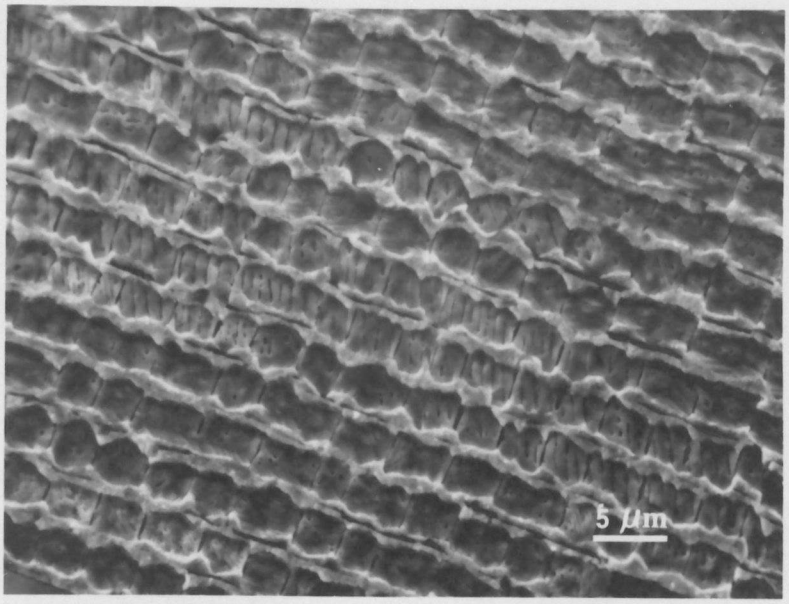
In-Sn-Cd

To help characterize the structure of the In-Sn-Cd-Zn eutectic, several ingots of the In-Sn-Cd ternary were directionally solidified to examine the microstructure of the coupled ternary eutectic.

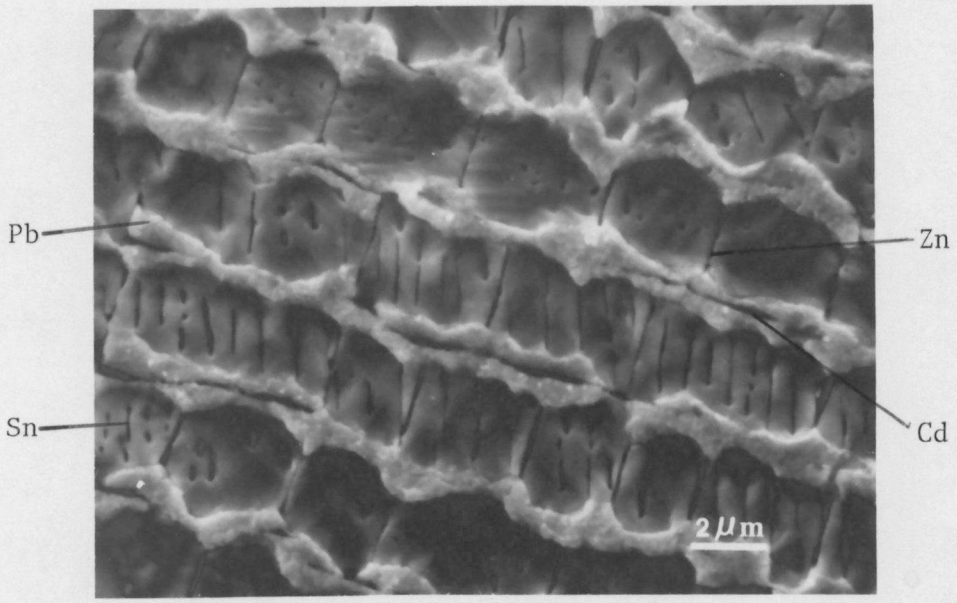
The coupled ternary structure consists of In and Sn rich phases in a lamellar array with the Cd phase also lamellar and perpendicular to the first two phases. The Cd rich phase is almost entirely contained within the In rich phase. This structure corresponds to the one reported by Cooksey and Hellawell[31]. The structure is shown in Figure 8.

In-Sn-Cd-Zn

Figure 9 shows the structure of the coupled four phase In-Sn-Cd-Zn eutectic. The coupled In-Sn-Cd ternary structure is retained.

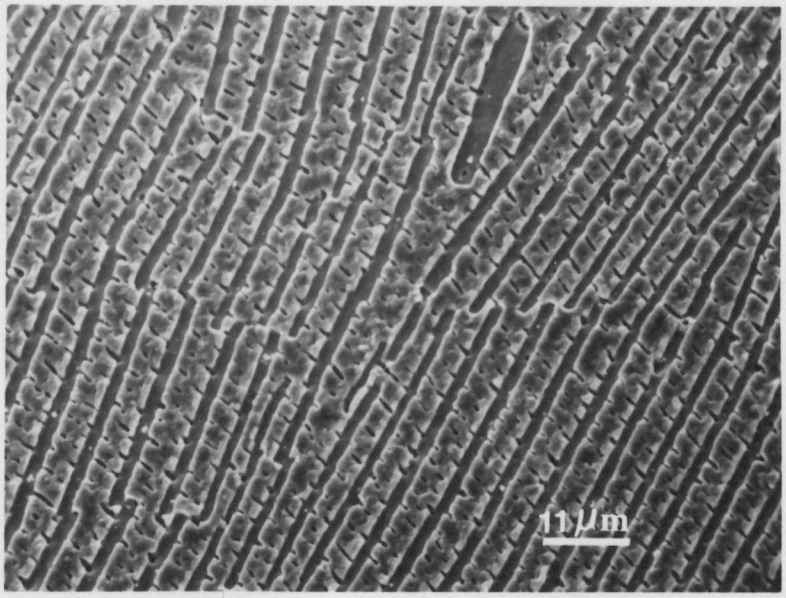


(a) Ingot 1090, R = 2.44 x 10^{-4} cm/sec.

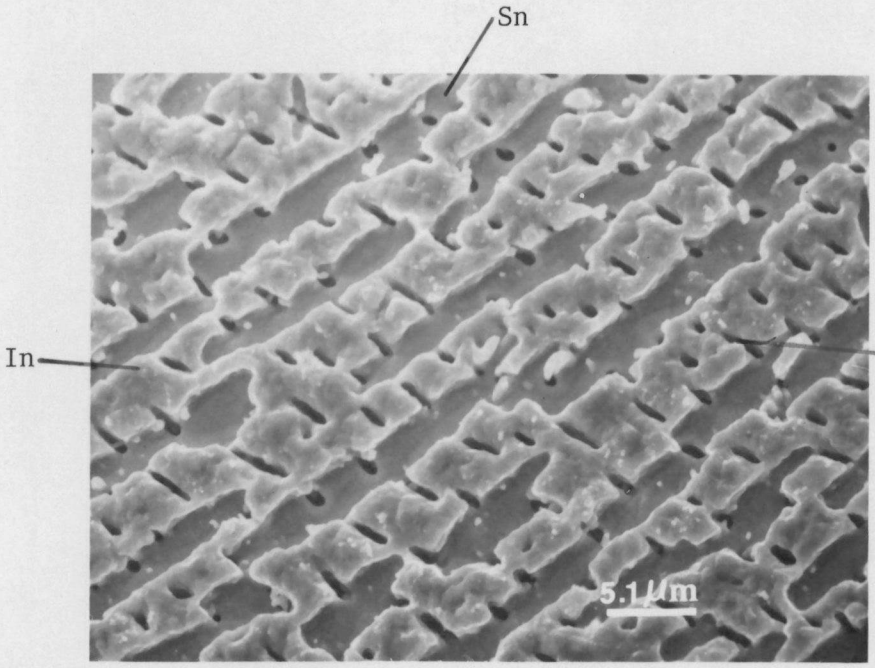


(b) Ingot 1090, R = 2.44 x 10^{-4} cm/sec.

Figure 7. Coupled Pb-Sn-Cd-Zn eutectic.

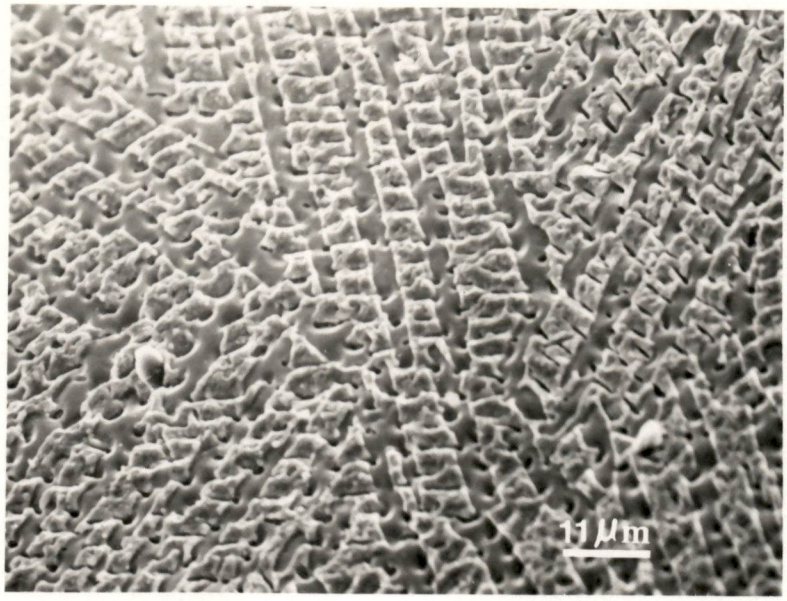


(a) Ingot 1052, R = 6.0×10^{-4} cm/sec.

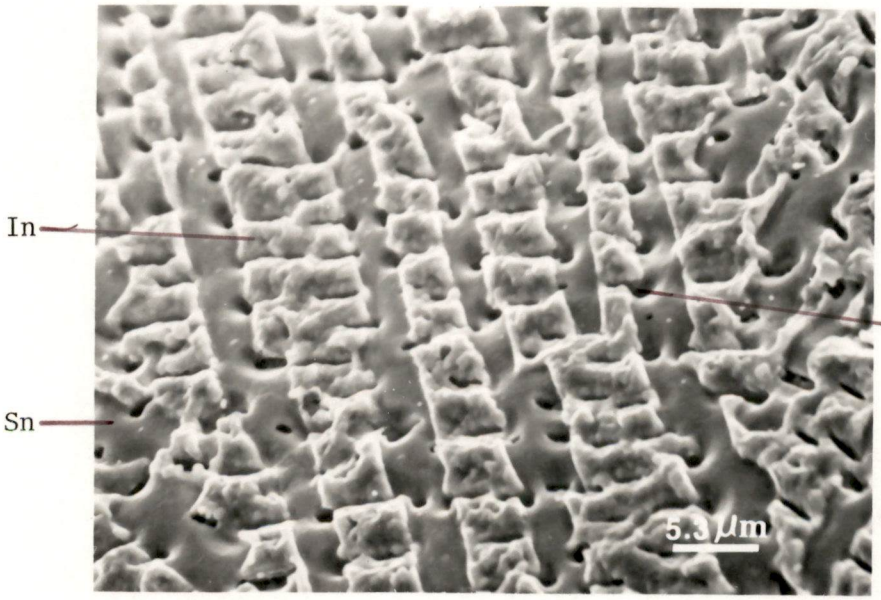


(b) Ingot 1052, R = 6.0×10^{-4} cm/sec.

Figure 8. Coupled In-Sn-Cd eutectic.



(a) Ingot 1070, R = 2.16×10^{-4} cm/sec.



(b) Ingot 1070, R = 2.16×10^{-4} cm/sec.

Figure 9. Coupled In-Sn-Cd-Zn eutectic.

Dispersive X-ray analysis in the SEM revealed that the Zn is contained within the Cd phase, but its morphology could not be determined because of its small volume fraction.

The quaternary eutectic exists for the following reasons:

1 the quaternary eutectic temperature of 86°C is lower than any of the four ternary eutectic temperatures of the system, and is the *minimum* temperature in the four component system where a liquid can exist,

2 the non-directional furnace cooling curves of the quaternary showed a thermal *arrest* at 86°C, and

3 the thermal breaks in the directionally solidified quaternary ingots were measured as 86°C.

For both quaternary systems studied, the coupled morphology of the three highest volume phases is retained in the coupled four phase structure. The basic three phase morphology is retained because the addition of Zn to form the four phase eutectic did not significantly affect the diffusion of the other three components in the liquid in front of the interface or apparently alter the interfacial energy relations between the phases.

IV. REGION OF COUPLED GROWTH

Pb-Sn-Cd-Zn

Ingots at the Pb-Sn-Cd-Zn eutectic composition were coupled for all velocities examined. In order to examine the region of compositions about the eutectic where coupled growth might occur, four ingots of off-eutectic composition were directionally solidified.

The ingots were 5 wt% richer than the eutectic composition in each of the four components. The compositions, growth conditions and observed microstructures are listed in Table IV of the Appendix.

The Sn rich ingot (Ingot 1098) was coupled for G/R values greater than 6×10^5 C-sec/cm^2 and the Pb rich ingot (Ingot 1102) was coupled for G/R between 7×10^5 and 19×10^5 C-sec/cm^2. The other two ingots were totally dendritic. The volume of compositions where coupled growth occurs expands towards the Sn and Pb rich compositions as G/R increases. There is not enough data to exactly define the compositions where coupled growth can occur for a given G/R value, but the results show that this volume lies mainly within 5% of the eutectic compositon for the G/R values examined.

In-Sn-Cd-Zn

Ingots at the published In-Sn-Cd-Zn eutectic composition were coupled for values of G/R between 1.2×10^5 and 1.5×10^5 C-sec/cm^2, and greater than 9×10^5 C-sec/cm^2. All other G/R values were dendritic.

Again, four ingots of off-eutectic composition were examined. The ingots were 5 wt% richer than the eutectic composition in each of the components. The In rich ingot (Ingot 1078) was coupled for all G/R values investigated. The other three ingots were dendritic. Table V, in the Appendix, lists the compositions, growth conditions and the microstructures observed in these ingots.

The volume of compositions where coupled growth can occur is bounded within 5% of the eutectic in the Sn, Cd and Zn rich direc-

tions but opens up towards the In rich compositions. The extent of this volume of compositions in the In rich direction was not determined.

V. EXTREMUM CONDITION

The two quaternaries obey the $\lambda^2 R$ extremum condition for coupled growth. Measurements of the lamellar spacing of the interdendritic eutectic are also consistent with the extremum condition.

Pb-Sn-Cd-Zn

The measured lamellar spacings in the Pb-Sn-Cd-Zn ingots are shown in Figure 10. The measured values agree with those observed by Holder and Oliver[7] for the ternary Pb-Sn-Cd system. The lamellar spacing measured was the Sn-Pb-Cd-Pb-Sn spacing because it was more regular than the Zn-Sn-Zn spacing. The Zn-Sn-Zn spacing is, on the average, about 40% wider than the Sn-Pb-Cd-Pb-Sn spacing, which agrees with Fisher and Kurz's[24] observations. The measured values of the spacings do not agree numerically, however, with the values reported by Fisher and Kurz for the quaternary or by Bao and Durand[21] for the ternary. It is interesting to note that the last two works agree with each other.

There was a significant difference in the temperature gradients used in the different studies. Gradients of 250 to 400 C/cm were used in both the present work and that of Holder and Oliver. Fisher and Kurz and Bao and Durand used gradients of 15 to 20 C/cm.

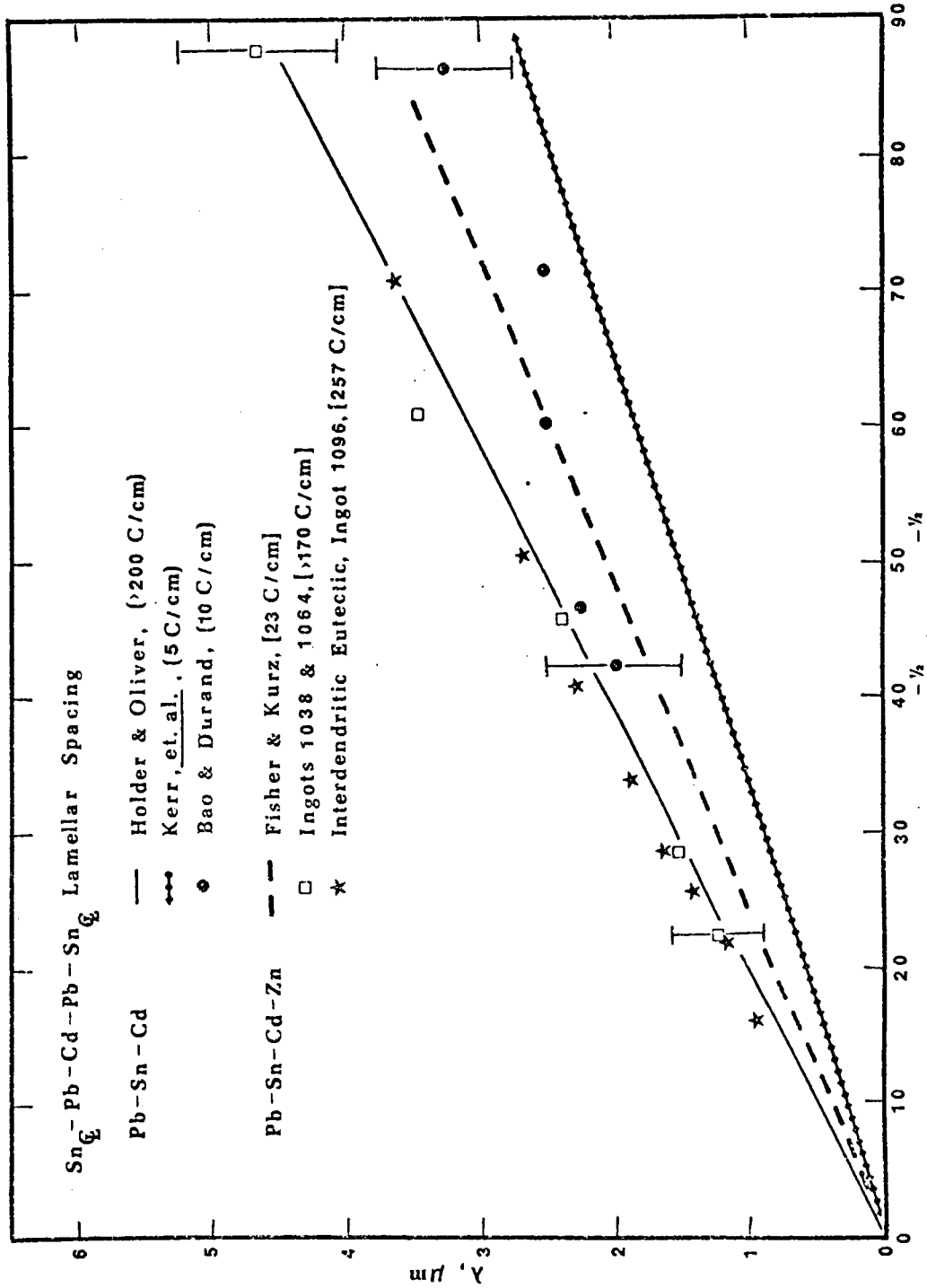


Figure 10. The variation of the lamellar spacing with velocity in the Pb-Sn-Cd-Zn system.

The temperature gradient was thought to have affected the lamellar spacings. It appeared that higher gradients resulted in wider spacings. The results of Kerr, Bell and Winegard[32], with a gradient of 5 C/cm, added weight to the hypothesis (see Figure 10).

To test the hypothesis, two ingots of the Pb-Sn-Cd ternary eutectic were solidified at different thermal gradients. The two ingots were drawn from the same melt to eliminate any effect of volume fractions on the lamellar spacing. One ingot was solidified with a gradient of 31.1 C/cm (Ingot 1092) and the other with a gradient of 386 C/cm (Ingot 1094).

The lamellar spacings of the two ingots are shown in Figure 11. There are no significant differences in the measured spacings for the two ingots. It was concluded that the thermal gradient had no significant effect on the lamellar spacings, and that the variations in the results are somehow due to differences in experimental procedures and equipments.

In-Sn-Cd-Zn

Figure 12 shows the results for the In-Sn-Cd-Zn alloys. The Sn-In-Sn spacing was measured because it was more regular and definite than the Cd-In-Cd spacing. On the average, the Cd-In-Cd spacing is about 40 to 50% of the Sn-In-Sn spacing. The addition of Zn did not visibly affect the Sn-In-Sn spacing in the quaternary as compared to the ternary.

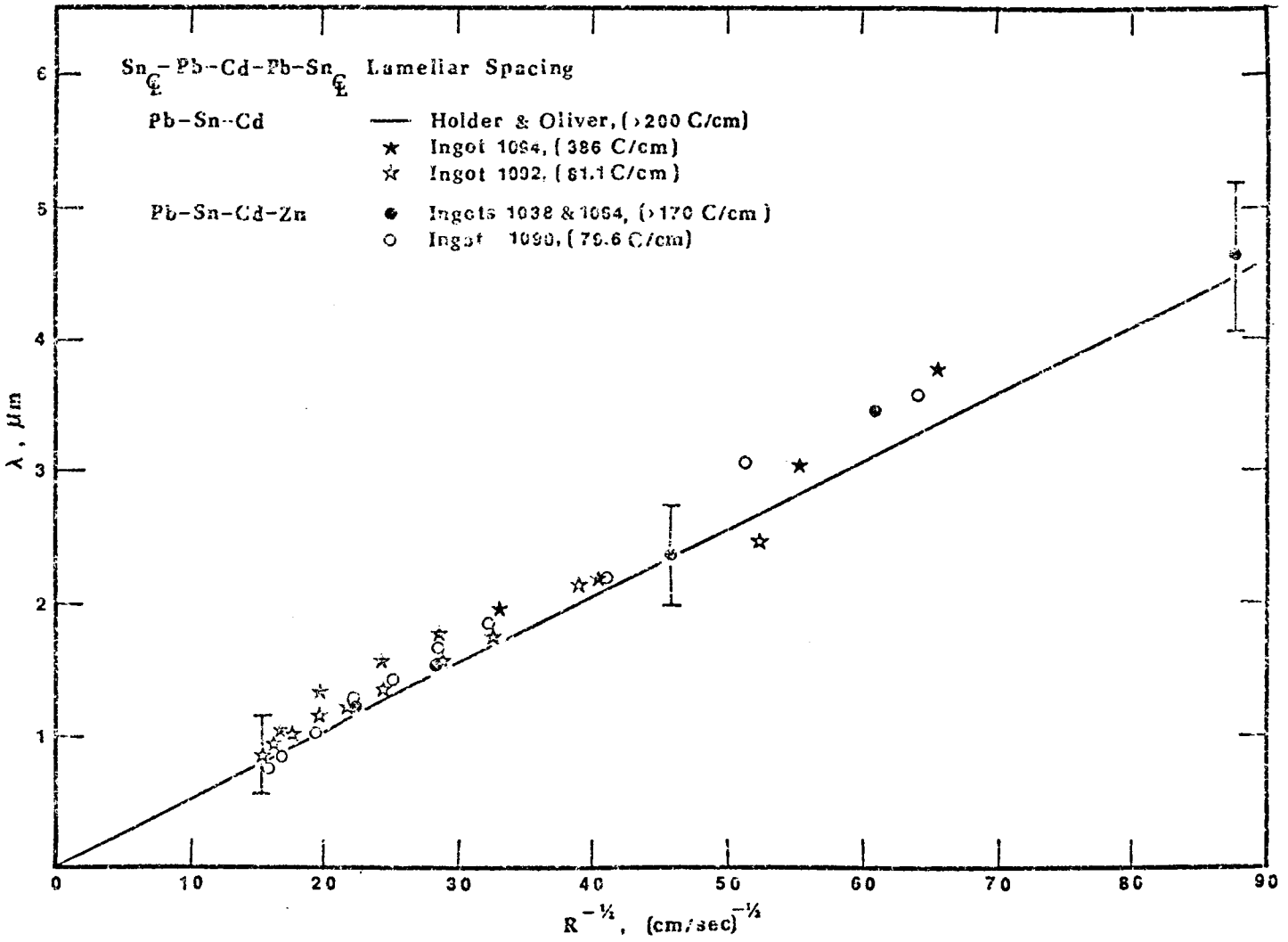


Figure 11. Lamellar spacing of the high and low gradient Pb-Sn-Cd-Zn alloys.

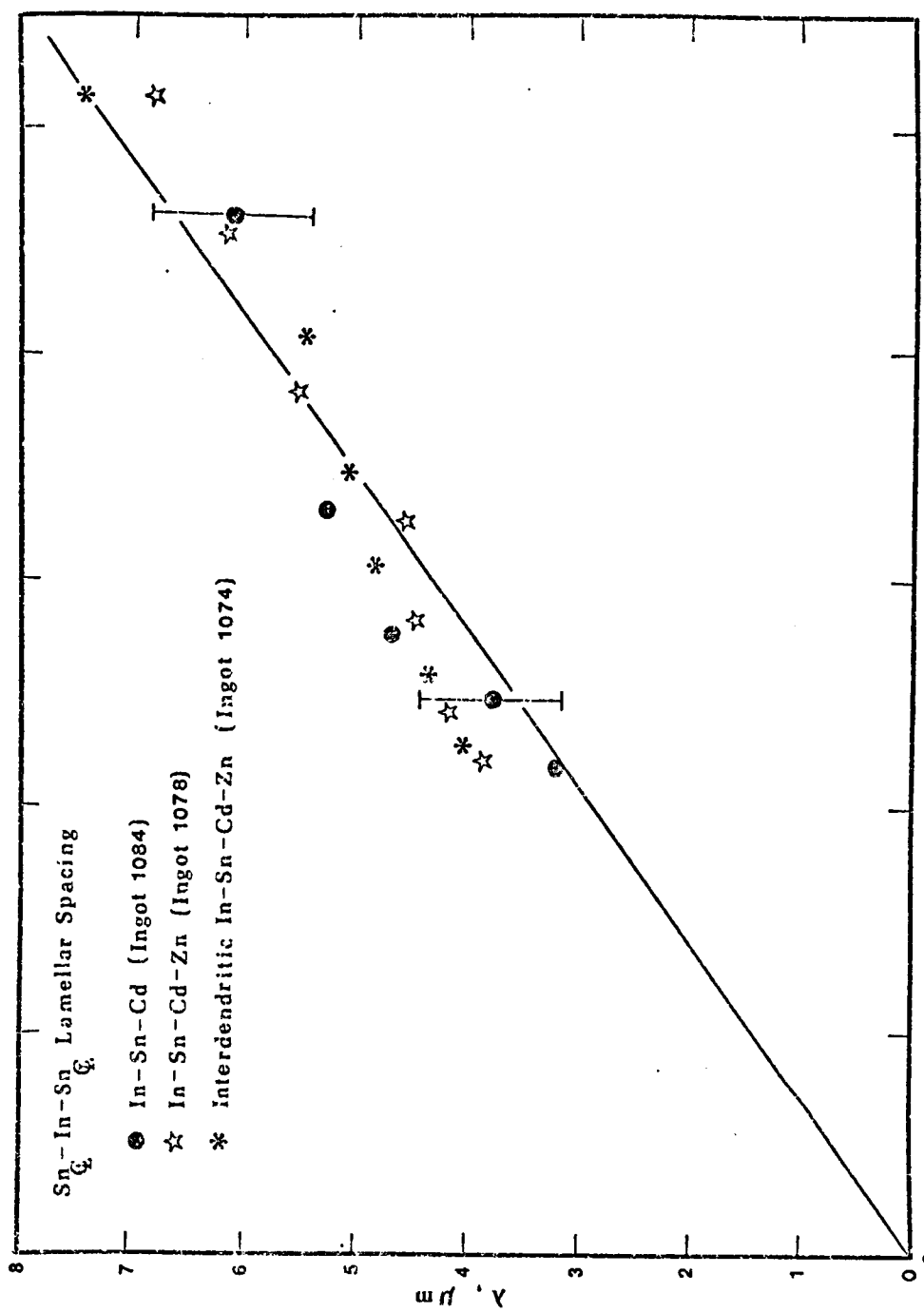


Figure 12. The variation of the lamellar spacing with velocity in the In-Sn-Cd-Zn system.

VI. DENDRITE STRUCTURES

Dendrites occured in the specimens when the conditions for directional solidification were such that a planar interface was no longer stable. As noted previously, the temperature profile of the ingots was a good indicator of the presence of dendrites. When the thermal break was sharp, the structures were coupled. When the thermal break was rounded or when two thermal breaks were observed, dendrites were observed in the specimens. When two thermal breaks were observed, the higher temperature corresponded to the liquidus temperature and the lower temperature was always the eutectic temperature.

Types of Dendrites

The two quaternaries were not studied in detail. The observed dendrites do not represent all the possible dendrites that could occur in the systems.

Pb-Sn-Cd-Zn. The dendrites occuring in the Pb-Sn-Cd-Zn system are shown in Figure 13. They are the:

1 Zn rich single phase dendrites (Figures 13 a and b),

2 Sn rich single phase dendrites (Figures 13 c and d),

3 Pb rich single phase dendrites (Figures 13 e and f),

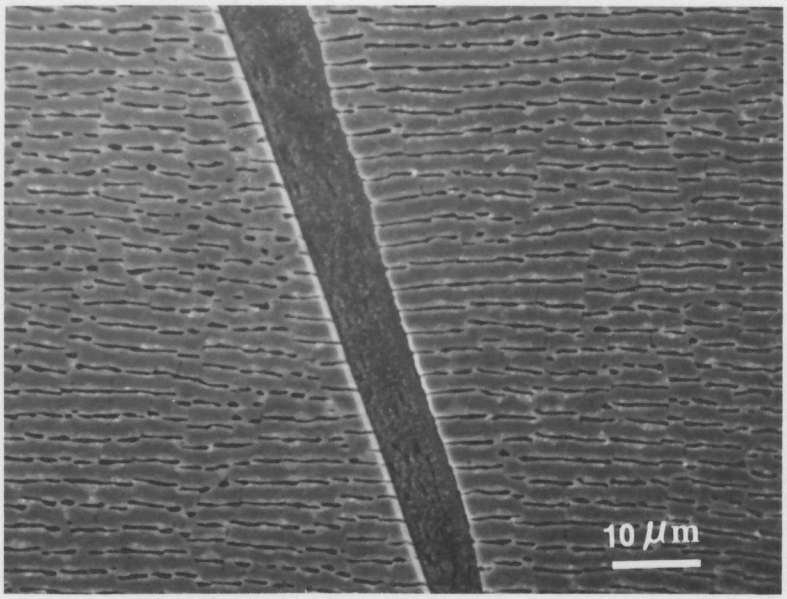
4 Cd rich single phase dendrites (Figures 13 g and h),

5 Pb-Sn-Zn three phase dendrites (Figures 13 i and j), and

6 Pb-Sn-Cd three phase dendrites (Figures 13 k and l).

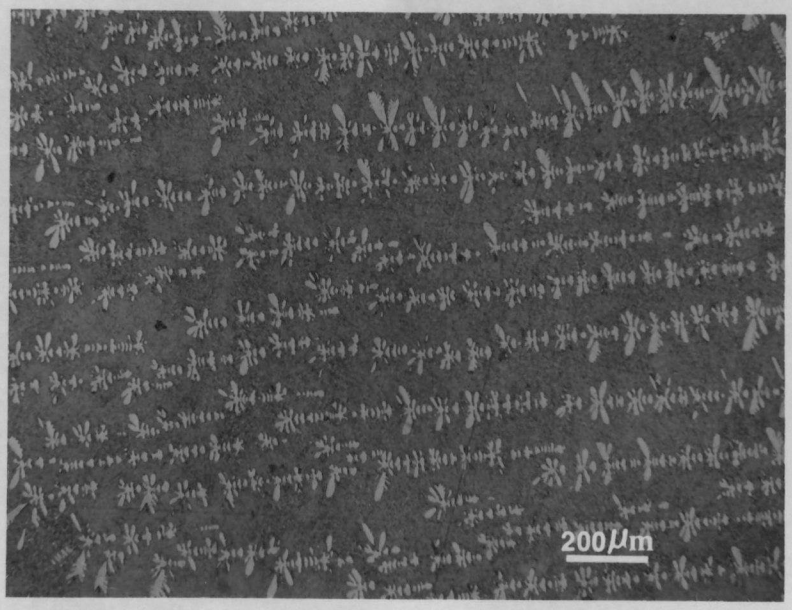


(a) Zn dendrites in Pb-Sn-Cd-Zn matrix, Ingot 1096, $R = 3.95 \times 10^{-4}$ cm/sec.

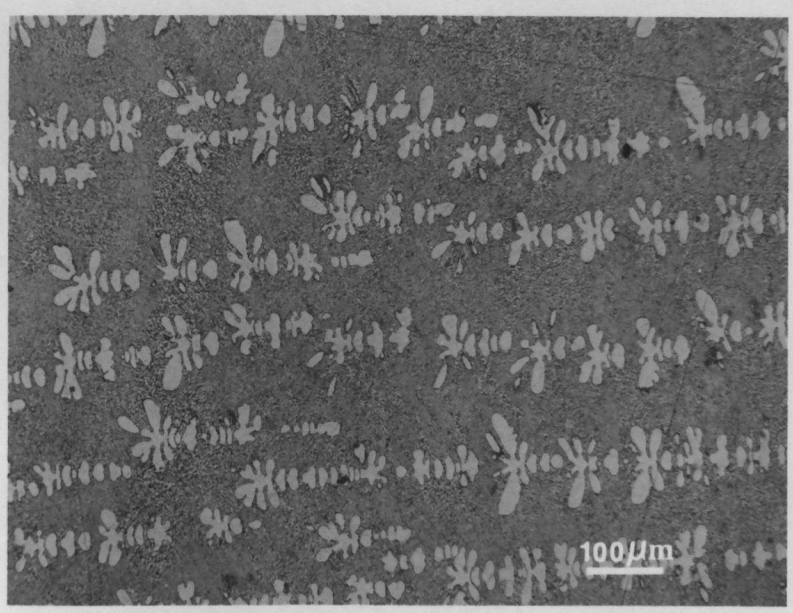


(b) Zn dendrite in Pb-Sn-Cd-Zn matrix, Ingot 1096, $R = 3.95 \times 10^{-4}$ cm/sec.

Figure 13. Dendrites in the Pb-Sn-Cd-Zn quaternary.

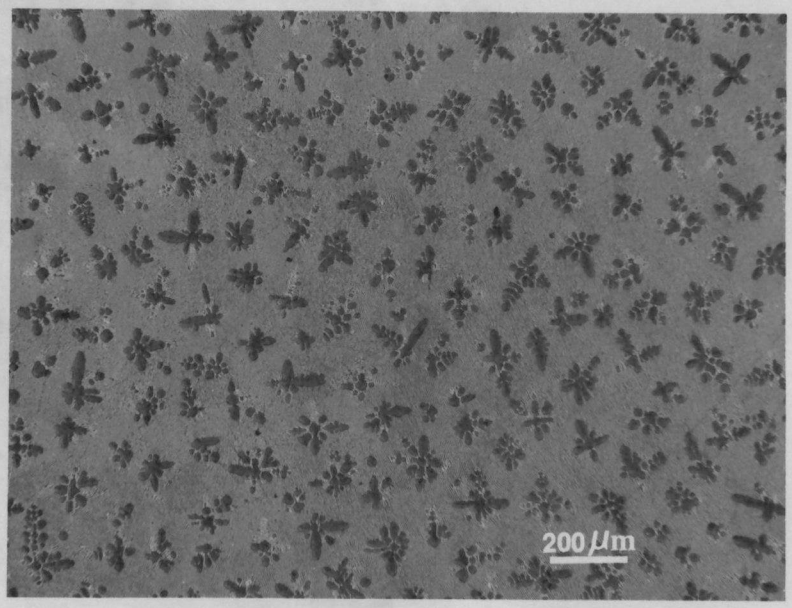


(c) Sn dendrites in Pb-Sn-Cd-Zn matrix, Ingot 1098, $R = 39.8 \times 10^{-4}$ cm/sec.

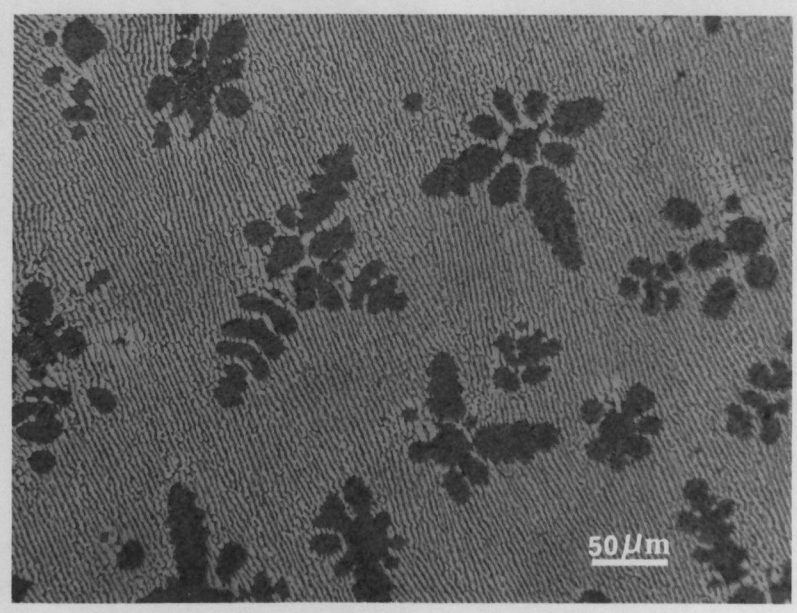


(d) Sn dendrites in Pb-Sn-Cd-Zn matrix, Ingot 1098, $R = 39.8 \times 10^{-4}$ cm/sec.

Figure 13. (continued)

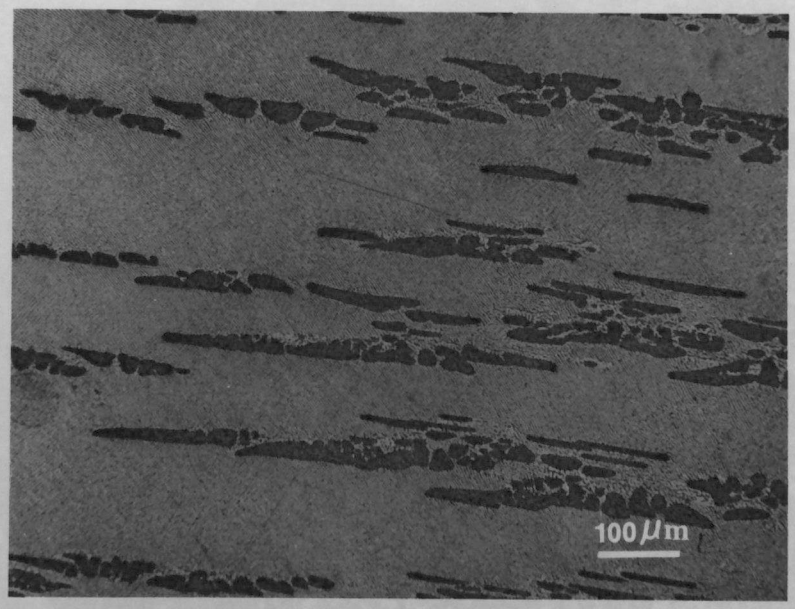


(e) Pb dendrites in Pb-Sn-Cd-Zn matrix, Ingot 1102, R = 1.99 x 10^{-4} cm/sec.

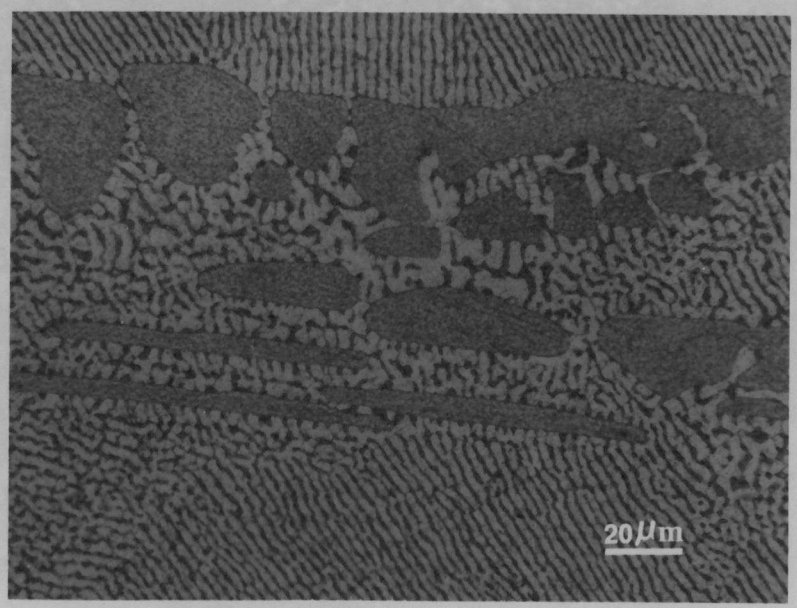


(f) Pb dendrites in Pb-Sn-Cd-Zn matrix, Ingot 1102, R = 1.99 x 10^{-4} cm/sec.

Figure 13. (continued)

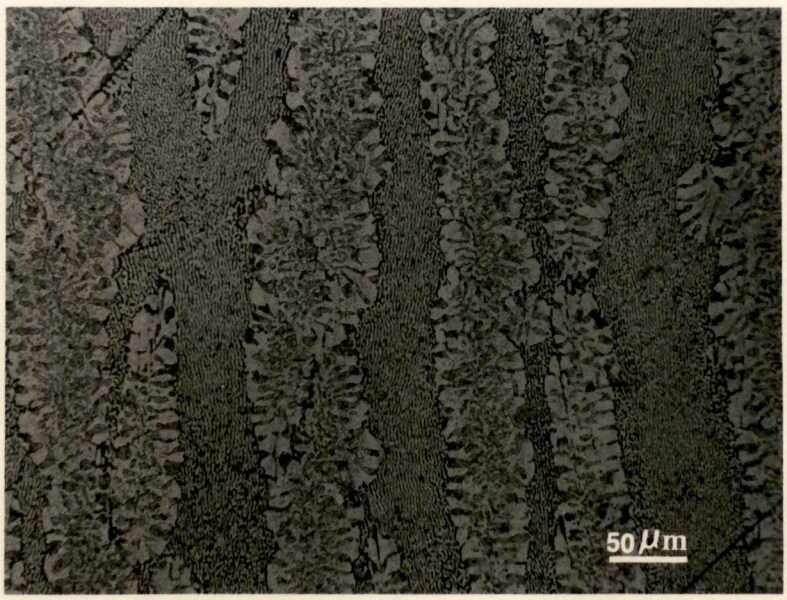


(g) Cd dendrites in Pb-Sn-Cd-Zn matrix, Ingot 1100, R = 3.77×10^{-4} cm/sec.

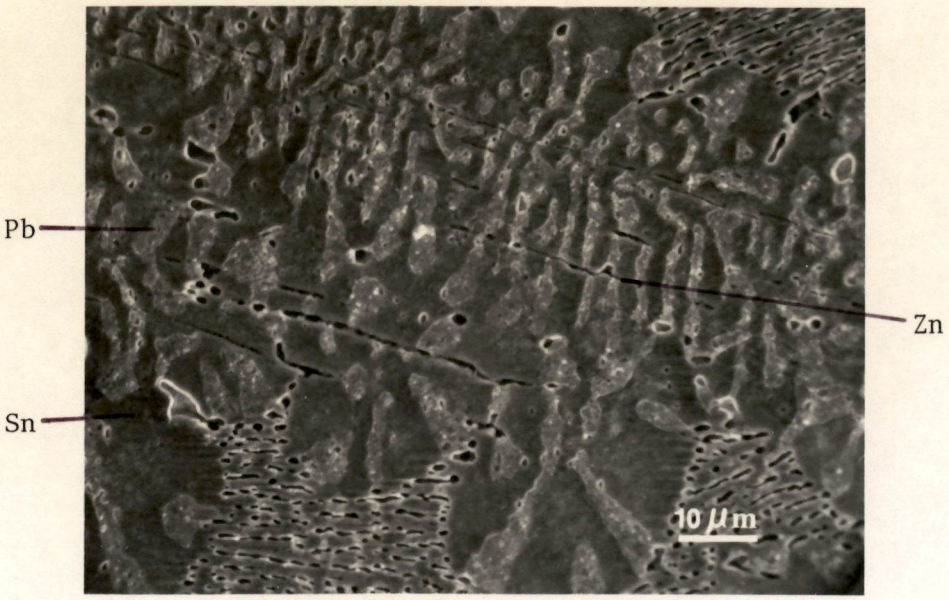


(h) Cd dendrites in Pb-Sn-Cd-Zn matrix, Ingot 1100, R = 3.77×10^{-4} cm/sec.

Figure 13. (continued)

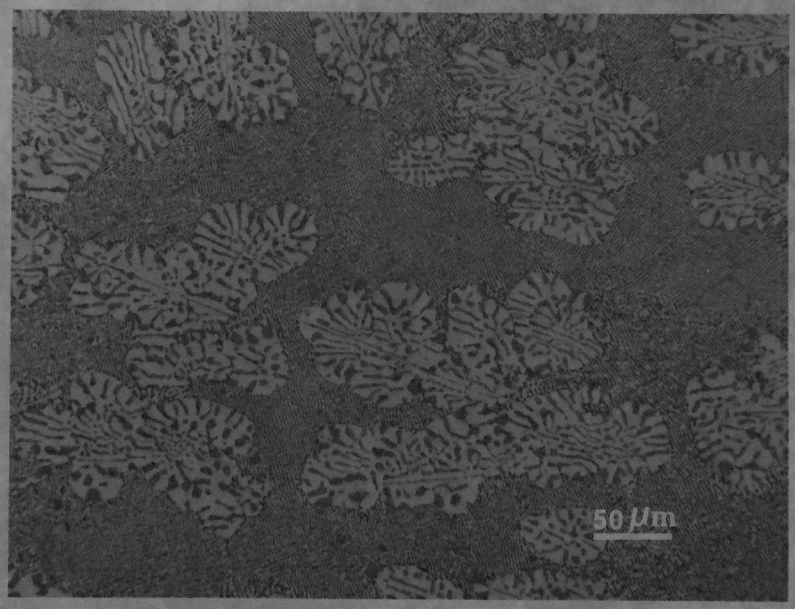


(i) Pb-Sn-Zn dendrites in Pb-Sn-Cd-Zn matrix, Ingot 1096, R = 6.01 x 10^{-4} cm/sec.

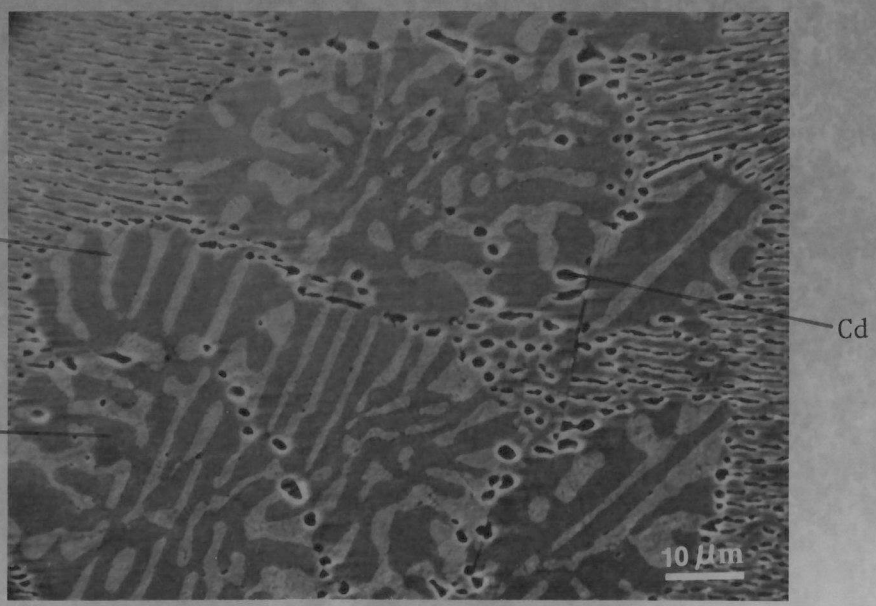


(j) Pb-Sn-Zn dendrite in Pb-Sn-Cd-Zn matrix, Ingot 1096, R = 6.01 x 10^{-4} cm/sec.

Figure 13. (continued)



(k) Pb-Sn-Cd dendrites in Pb-Sn-Cd-Zn matrix, Ingot 1100, R = 9.07 x 10^{-4} cm/sec.



(l) Pb-Sn-Cd dendrite in Pb-Sn-Cd-Zn matrix, Ingot 1100, R = 9.07 x 10^{-4} cm/sec.

Figure 13. (continued)

In-Sn-Cd. Several dendrites were observed in the In-Sn-Cd ternary. They are shown in Figure 14 and are the:

1 Cd rich single phase dendrites (Figures 14 a and b),

2 Sn rich single phase dendrites (Figures 14 c and d), and

3 Sn-Cd two phase dendrites (Figures 14 e and f).

In-Sn-Cd-Zn. The dendrites found in the In-Sn-Cd-Zn system are shown in Figure 15. They are the:

1 Sn rich single phase dendrites (Figures 15 a and b),

2 Cd-Sn two phase dendrites (Figures 15 c and d),

3 Zn-In two phase dendrites (Figures 15 e and f), and

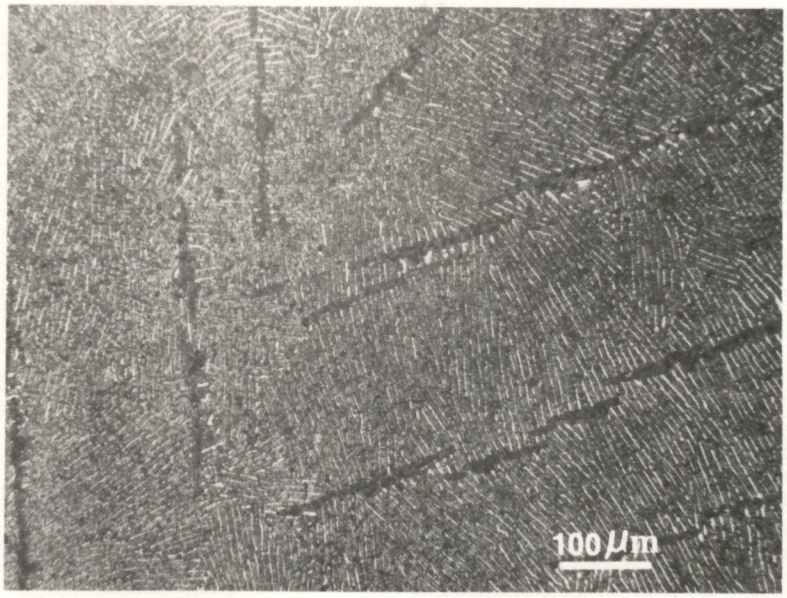
4 In-Sn-Cd three phase dendrites (Figures 15 g and h).

Spatial Relationships of Multiphase Dendrites

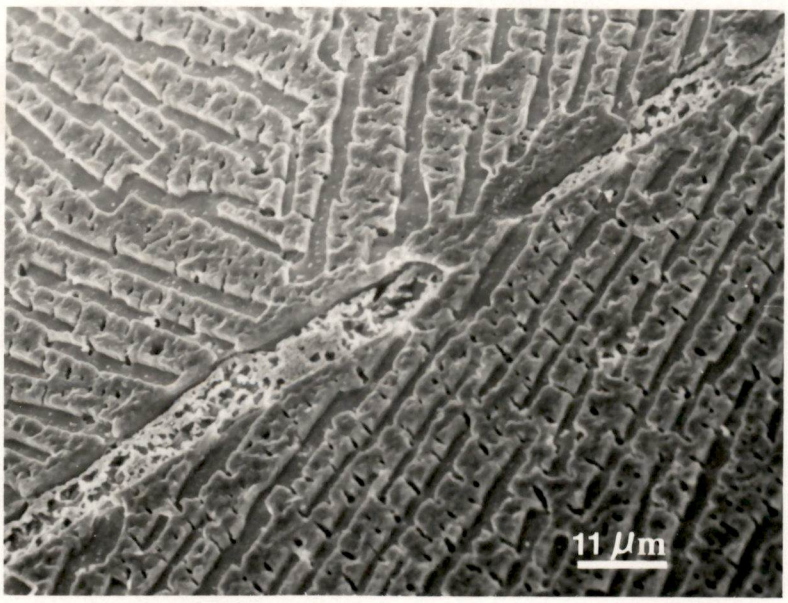
The multiphase dendrites solidify as a unit and are characterized by distinct spatial relationships between the phases.

Pb-Sn-Cd-Zn. The Pb-Sn-Zn dendrite (Figures 13 i and j) is an elongated dendrite composed of a flowery Sn phase with an interior skeletal network of Pb. The Zn forms as long thin sheets running along the spine of the dendrite.

The Pb-Sn-Cd dendrite (Figures 13 k and l) has the same Sn and Pb arrangement as the Pb-Sn-Zn dendrite. The Cd phase appears to be discontinuous and is found to be associated with the Pb phase. This may be due to the relatively high Sn-Cd interfacial energy (see Table I, page 6).

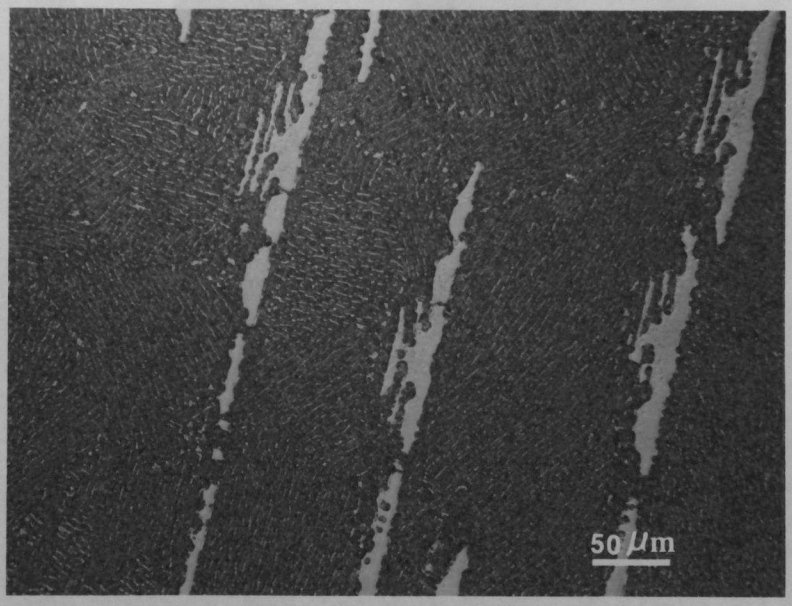


(a) Cd dendrites in In-Sn-Cd matrix, Ingot 1050, $R = 4.55 \times 10^{-4}$ cm/sec.

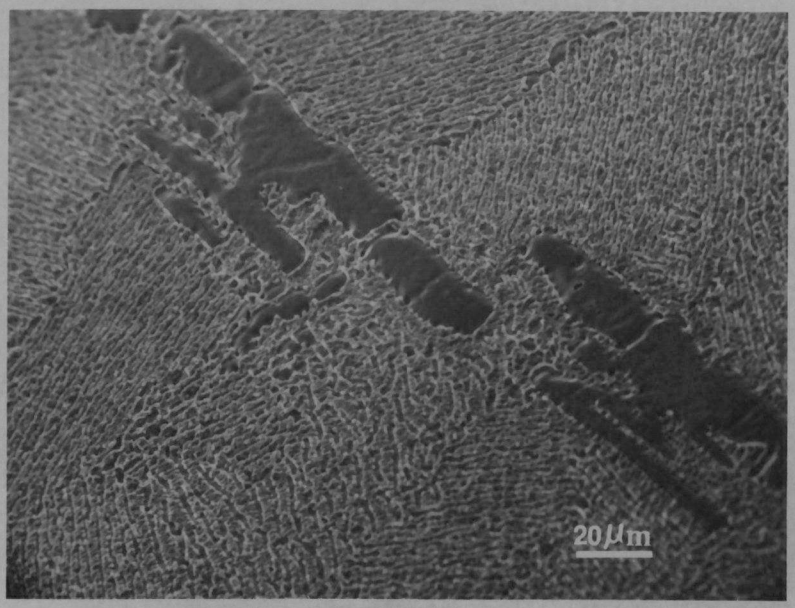


(b) Cd dendrite in In-Sn-Cd matrix, Ingot 1050, $R = 4.55 \times 10^{-4}$ cm/sec.

Figure 14. Dendrites in the In-Sn-Cd ternary.

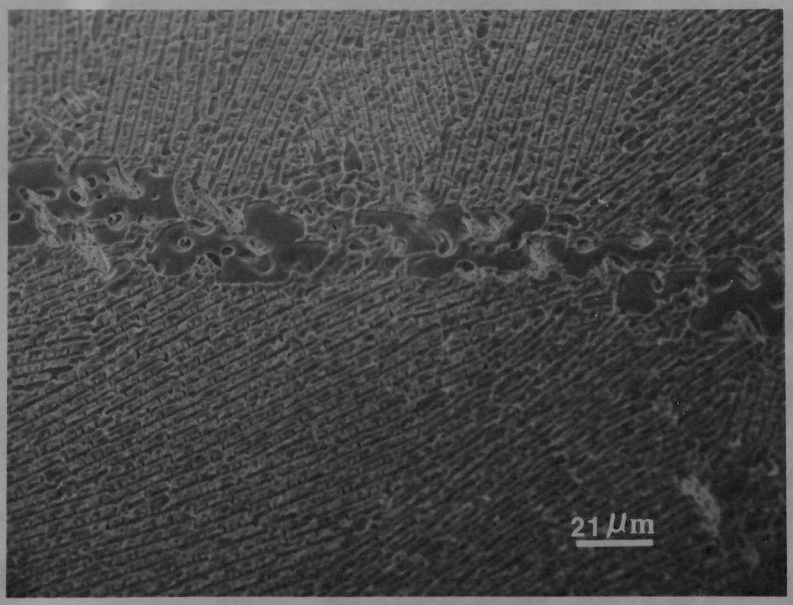


(c) Sn dendrites in In-Sn-Cd matrix, Ingot 1052, R = 18.3 x 10^{-4} cm/sec.

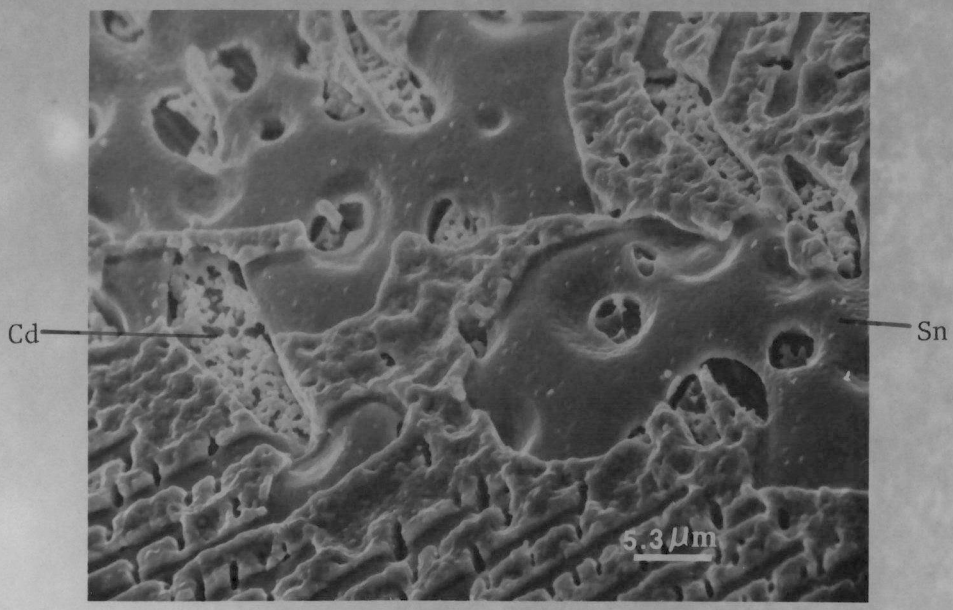


(d) Sn dendrites in In-Sn-Cd matrix, Ingot 1052, R = 18.3 x 10^{-4} cm/sec.

Figure 14. (continued)

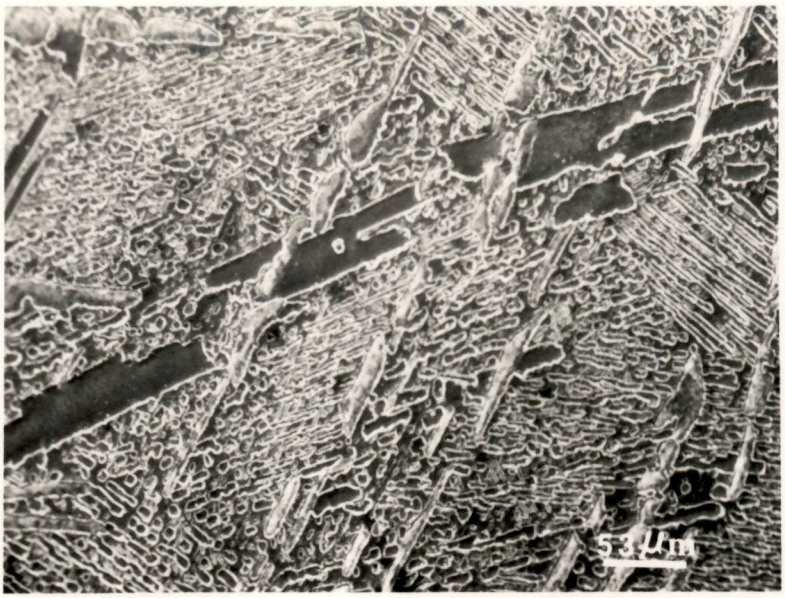


(e) Sn-Cd dendrite in In-Sn-Cd matrix, Ingot 1050, R = 14.7 x 10^{-4} cm/sec.

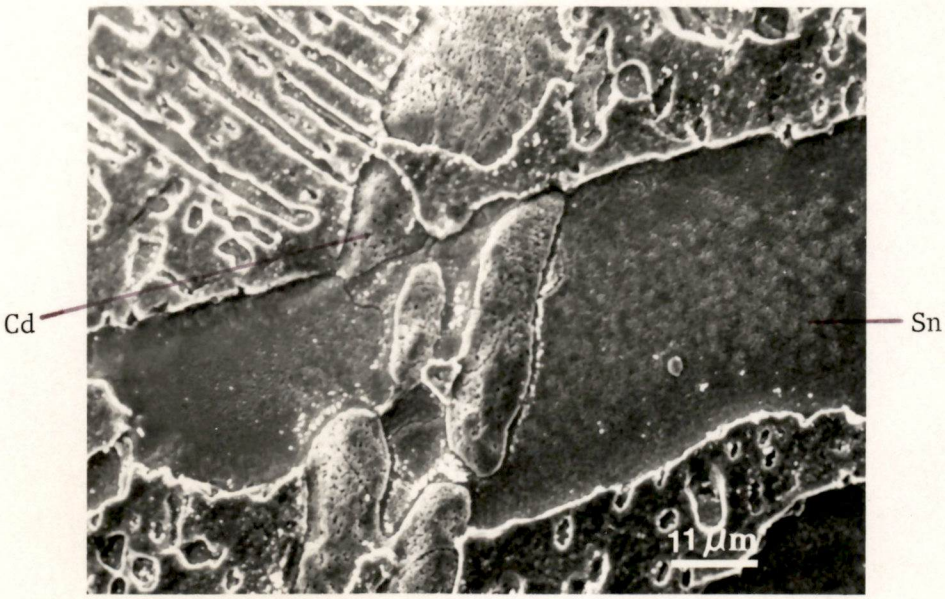


(f) Sn-Cd dendrite in In-Sn-Cd matrix, Ingot 1050, R = 14.7 x 10^{-4} cm/sec.

Figure 14. (continued)



(c) Cd-Sn dendrites in In-Sn-Cd-Zn matrix, Ingot 1076, R = 2.54 x 10^{-4} cm/sec.

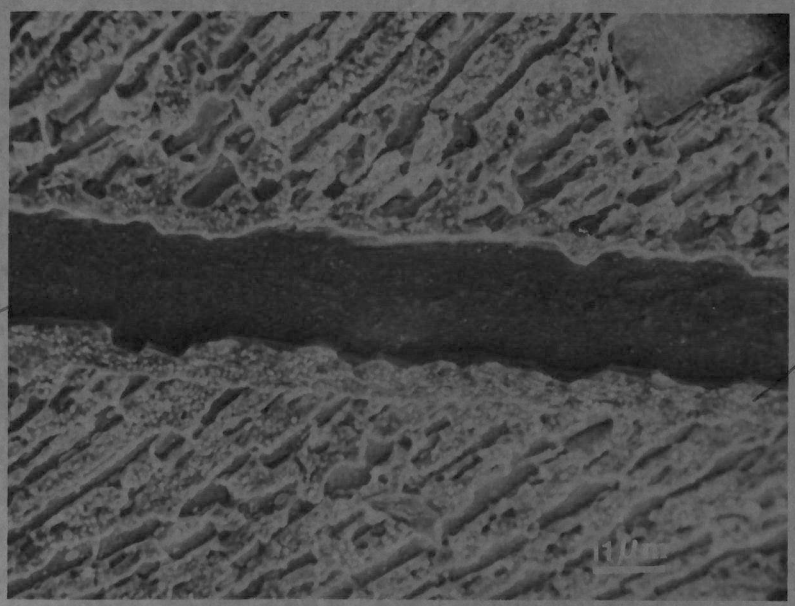


(d) Cd-Sn dendrite in In-Sn-Cd-Zn matrix, Ingot 1076, R = 2.54 x 10^{-4} cm/sec.

Figure 15. (continued)

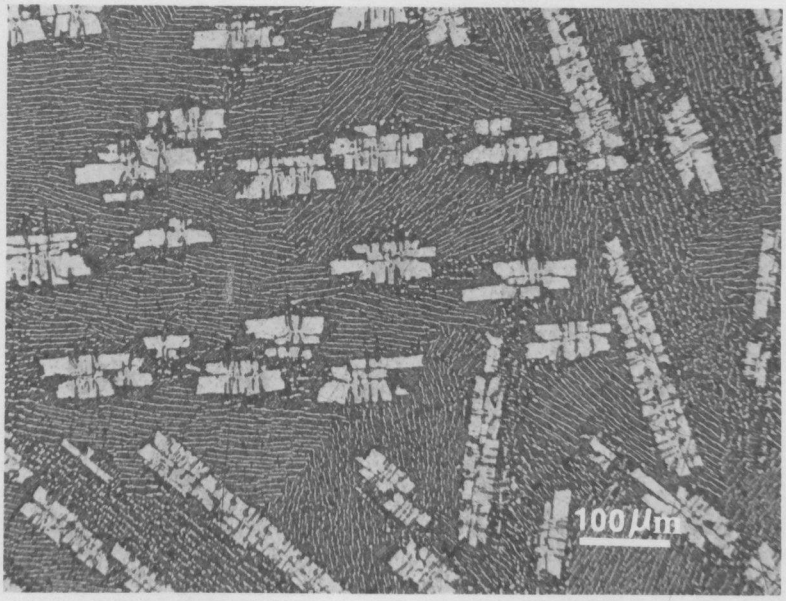


(e) Zn-In dendrites in In-Sn-Cd-Zn matrix, Ingot 1074, R = 2.37 x 10^{-4} cm/sec.

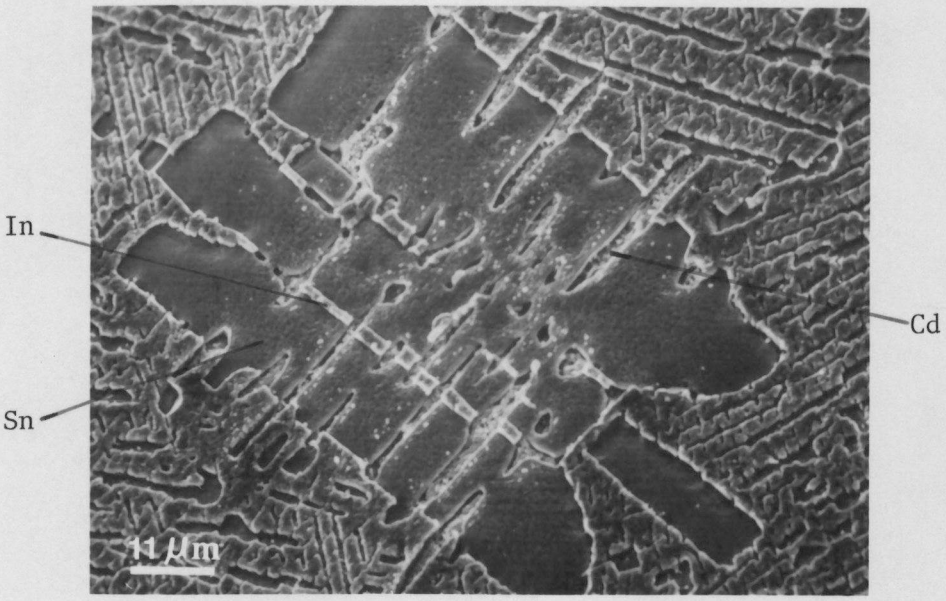


(f) Zn-In dendrite in In-Sn-Cd-Zn matrix, Ingot 1074, R = 2.37 x 10^{-4} cm/sec.

Figure 15. (continued)



(g) In-Sn-Cd dendrites in In-Sn-Cd-Zn matrix, Ingot 1072, R = 8.07 x 10^{-4} cm/sec.



(h) In-Sn-Cd dendrite in In-Sn-Cd-Zn matrix, Ingot 1072, R = 8.07 x 10^{-4} cm/sec.

Figure 15. (continued)

In-Sn-Cd. The Sn-Cd dendrite (Figures 14 e and f) is composed of a flowery Sn phase with teardrop shaped Cd phases attached to it. The Cd phase extends into the eutectic matrix and its area of contact with Sn appears to be minimized. Again, this may be due to the high Sn-Cd interfacial energy.

In-Sn-Cd-Zn. The Cd-Sn dendrite (Figures 15 c and d) is composed of long thin Sn and Cd phases growing across each other at angles of about 50° and 90° (over 90% of the dendrites have 50° between the phases). The contact area of the Sn and the Cd phases appears to be minimal.

The Zn-In dendrite (Figures 15 e and f) is composed of a sheet of Zn with an outer coating of In.

The In-Sn-Cd dendrite (Figures 15 g and h) is made up of a blocky Sn phase with sheets of In within the Sn. The In tends to separate the Sn into three (in general) rectangular sections. The Cd, found as long thin phases perpendicular the In phase, is attached to the Sn phase and grows out into the eutectic matrix. This is similar the the Cd phase of the Sn-Cd dendrite in the In-Sn-Cd ternary.

Path of Solidification

The types of dendrites present in the ingots show the path of solidification of the alloys. In general, the observed dendrites were consistent with the phase diagram. The path of solidification depends on the initial composition of the ingot and the growth conditions.

Composition Effects. An ingot whose composition passes through a primary phase region will form a primary, single phase solid when the liquidus temperature is reached. As the temperature is lowered, the liquid and solid compositions will follow the tie line relationships specified by the phase diagram. When the liquid is on a bivariant two solid phase surface, a second solid crystallizes. The liquid continues to change in composition on further solidification and when it reaches a composition on a monovariant three solid phase line, a third solid will form. The liquid will finally move to the invariant four solid phase composition, the eutectic composition, where all four solids form simultaneously from the liquid.

The leading phase in the dendritic ingots appears to be the primary phase. The thermal breaks in the ingots support this observation. The higher temparature break in the ingots with two thermal breaks coincides with the liquidus temperature, which is the temperature at which the primary phase begins to solidify from the melt. This means that the primary dendrites project out into the liquid ahead of the eutectic interface until the tips of the dendrites are at the liquidus temperature.

The distance the dendrites project into the liquid ahead of the eutectic can be calculated from the time interval between the two thermal breaks. The calculated values are shown in Table III. The dendrites in the In-Sn-Cd-Zn alloys extend two to three times further into the liquid than the dendrites of the Pb-Sn-Cd-Zn alloys because of the shallower gradients encountered in the In-Sn-Cd-Zn ingots.

TABLE III

EXTENSION OF DENDRITES AHEAD OF THE EUTECTIC INTERFACE

System	Ingot	Dendrite	Distance (mm)	G (C/cm)
Pb-Sn-Cd-Zn	1096 (Zn rich)	(Zn)	0.37	257
	1098 (Sn rich)	(Sn)	0.35	295
	1100 (Cd rich)	(Pb-Sn-Cd)	0.54	247
	1102 (Pb rich)	(Pb)	0.35	389
In-Sn-Cd-Zn	1074 (Zn rich)	(Zn)	----[a]	205
	1076 (Cd rich)	(Cd)	1.7	221
	1078 (In rich)	(coupled)	----	208
	1080 (Sn rich)	(Sn)	1.1	235

[a]Double temperature break not observed.

Ingots 1080 and 1102 follow similar solidification paths. Ingot 1080 is the Sn rich off-eutectic alloy in the In-Sn-Cd-Zn system. Figure 16 shows the microstructure of the ingot. The initial composition of the ingot places it within the Sn primary phase volume. Large Sn dendrites are observed in the ingot. During solidification, the dendrites project out into the liquid until the tips are at the liquidus temperature. As the Sn dendrite forms, the interdendritic liquid becomes depleted in Sn. The liquid composition changes until it is on the Sn-Cd bivariant surface. Cd solidifies at this point. The Cd is attached to the Sn and extends out into the interdendritic liquid. The liquid composition continues to change behind the dendrites and finally reaches the In-Sn-Cd monovariant line where the In-Sn-Cd three phase dendrites appear. The liquid then moves along the monovariant line until it is at the eutectic composition and the interdendritic four phase eutectic solidifies. A schematic of the solid-liquid interface of this ingot is shown in Figure 17.

Inogt 1102 is the Pb rich off-eutectic alloy in the Pb-Sn-Cd-Zn system. The microstructure is shown in Figure 18. The initial composition of the ingot was within the Pb primary phase volume. Upon solidification, the Pb dendrites form first. A halo of Sn forms around the Pb when the liquid composition reaches the Pb-Sn bivariant surface. When the liquid is on the Pb-Sn-Cd monovariant line, the Pb-Sn-Cd three phase dendrites form around the Sn. Finally, the four phase interdendritic eutectic solidifies.

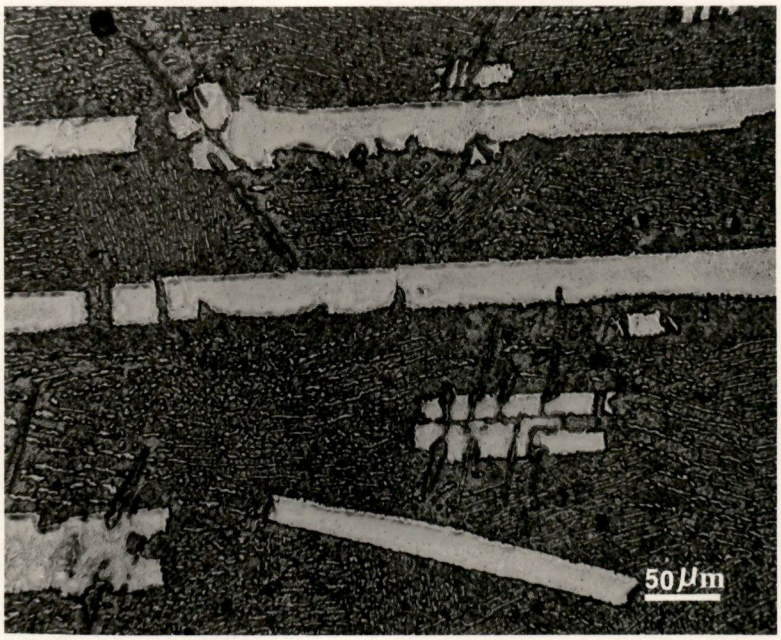


Figure 16. Typical microstructure of Ingot 1080.
$R = 3.05 \times 10^{-4}$ cm/sec.

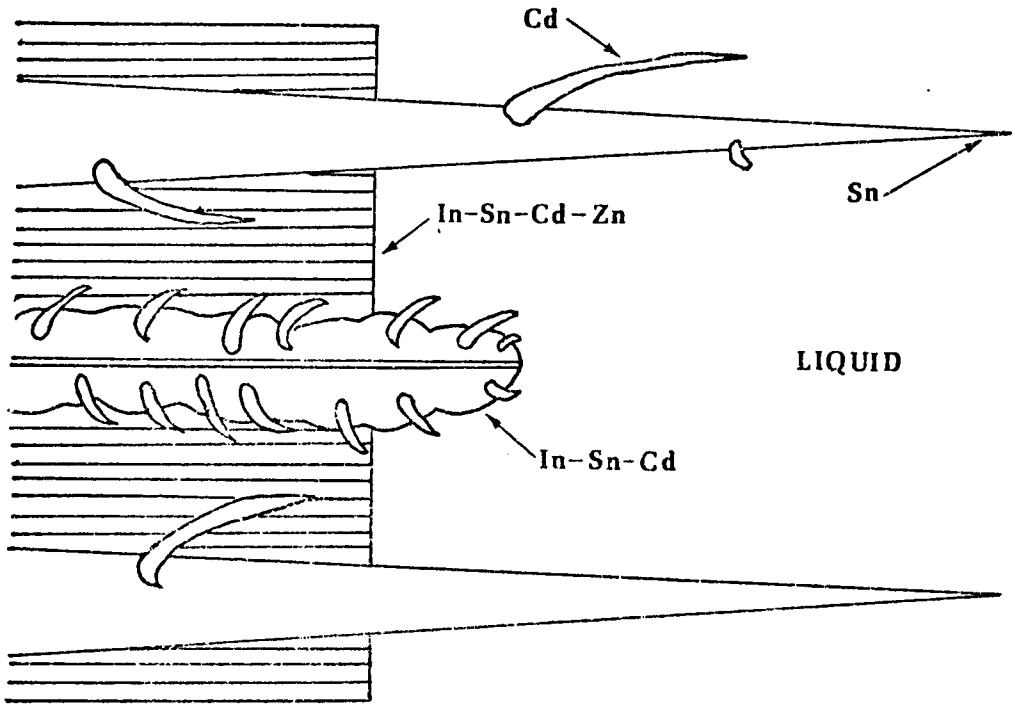


Figure 17. Schematic solid-liquid interface in Ingot 1080.

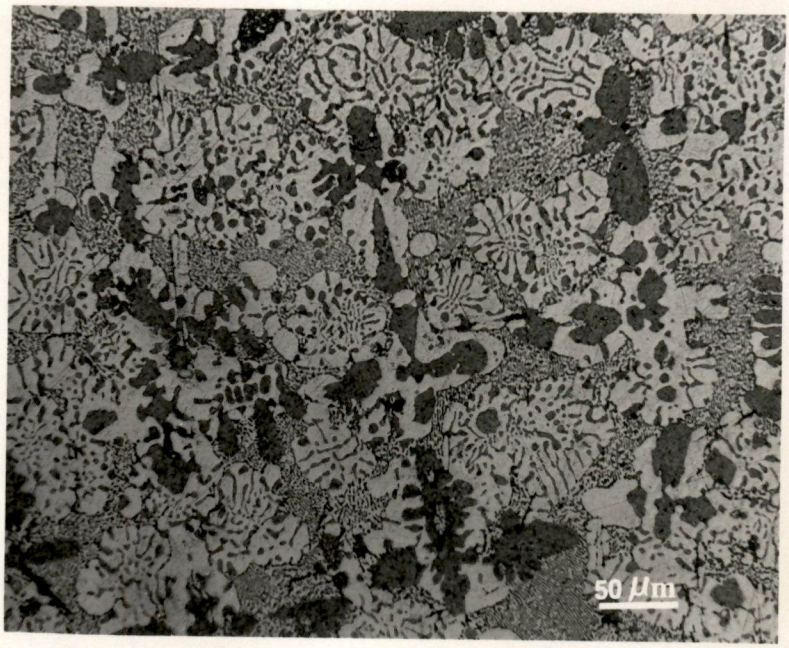


Figure 18. Typical microstructure of Ingot 1102.
$R = 15.7 \times 10^{-4}$ cm/sec.

Any of the steps in the solidification path described above may be bypassed during solidification depending on the composition of the ingot. For example, the liquid may move to a monovariant line without going through the bivariant surface. This occurs in Ingots 1098 (Sn rich in Pb-Sn-Cd-Zn) and 1096 (Zn rich in Pb-Sn-Cd-Zn). The structure of Ingot 1098 is shown in Figure 19. Upon solidification, Sn dendrites form first, followed by the Pb-Sn-Cd dendrites. In Ingot 1096 (Figure 20), the primary Zn dendrites solidified first. The three phase Pb-Sn-Zn dendrites then form around the Zn dendrites as soldification progresses without the intermediate two phase dendrites forming.

The liquid may also go directly to the eutectic composition from a bivariant surface without passing through a monovariant line. This is the case in Ingot 1076 (Cd rich in In-Sn-Cd-Zn) as shown in Figures 15 c and d. The Cd phase solidifies first, followed by the Sn, forming a two phase dendrite. The interdendritic liquid then forms the four phase eutectic without the appearance of an intermediate third phase.

Some specimens of the Cd rich ingot in the Pb-Sn-Cd-Zn system, Ingot 1100, solidified without any single or two phase dendrites. The three phase Pb-Sn-Cd dendrites were the only dendrites present, followed by the interdendritic quaternary eutectic (Figures 13 k and l).

Ingot 1074, the Zn rich ingot in the In-Sn-Cd-Zn system, follows an apparently discontinuous path of solidification. A typical microstructure is shown in Figure 21. During solidification, the primary Zn dendrites lead the solid interface. The interdendritic liquid



Figure 19. Typical microstructure of Ingot 1098.
$R = 8.93 \times 10^{-4}$ cm/sec.

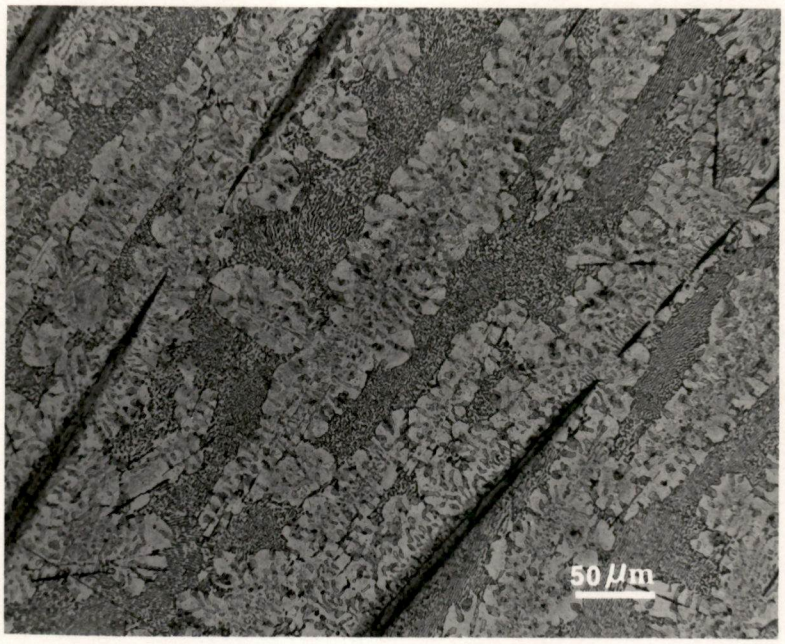


Figure 20. Typical microstructure of Ingot 1096.
$R = 15.6 \times 10^{-4}$ cm/sec.

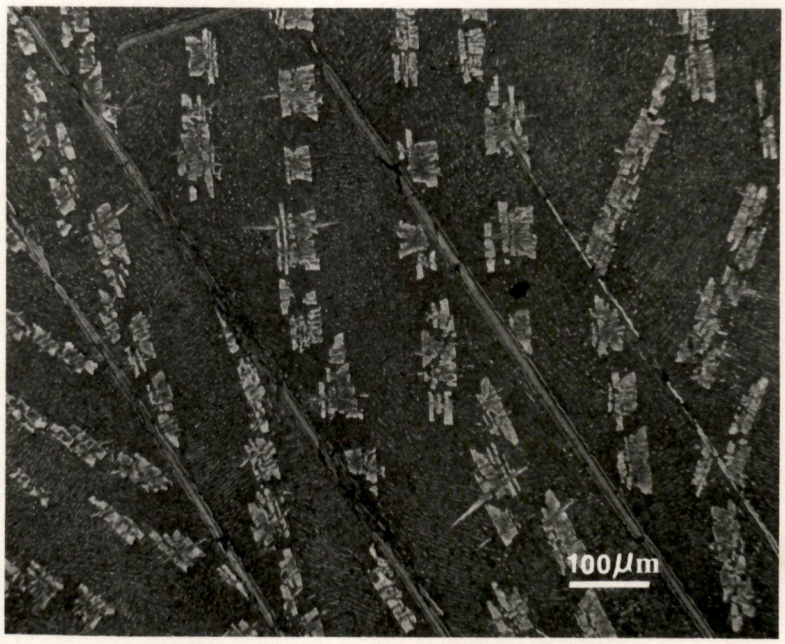


Figure 21. Typical microstructure of Ingot 1074.
$R = 14.8 \times 10^{-4}$ cm/sec.

changes composition until it reaches the Zn-In bivariant surface where a coat of In forms around the Zn dendrites (Figure 15 f). From here, the interdendritic liquid should continue to change composition until it either reaches one of the two monovariant lines that are at the boundary of the Zn-In bivariant surface, the Zn-In-Sn or the Zn-In-Cd monovariant lines, or until it is at the quaternary eutectic composition. The appearance of the In-Sn-Cd dendrites indicates the liquid composition to be on the In-Sn-Cd monovariant line instead of the expected ones.

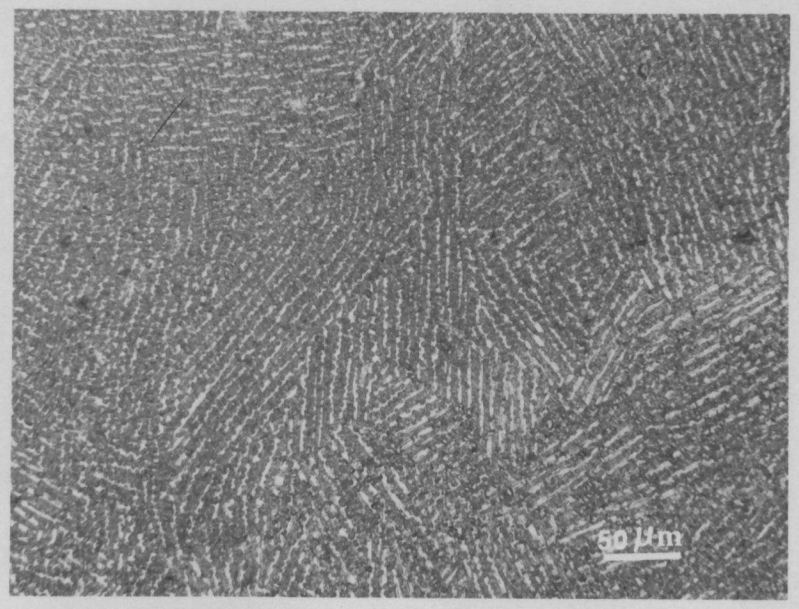
The solidus of a solidifying phase may show a decreasing solubility with decreasing temperature. This means that the amount of primary solid in equilibrium with the liquid may *decrease* with decreasing temperature. Of particular interest is the Cd-Zn binary[33] in which the Zn rich phase shows such a regression in its solidus just above the eutectic temperature. It is possible that the Zn rich phase of the quaternary In-Sn-Cd-Zn system may exhibit a similar behavior. The primary Zn dendrite leads the solid interface during solidification. The In phase forms a coat around the Zn when the liquid composition is on the Zn-In bivariant surface. As the temperature reaches the eutectic temperature in the interdendritic liquid, the liquid may want to redissolve some of the primary Zn phase due to the decreasing solubility of the other components in the Zn phase. The coating of In, however, effectively isolates the Zn phase from further participation in the solidification process. Because of the isolation of the Zn, the interdendritic liquid may also contain less Zn than the eutectic composition. The composition of the interden-

dritic liquid cannot stay on the Zn-In bivariant surface because the liquid is no longer in equilibrium with both the Zn and In phases. The liquid composition thus can follow the apparently discontinuous path out of the Zn-In bivariant surface on to the In-Sn-Cd monovariant line where the three phase In-Sn-Cd dendrites form.

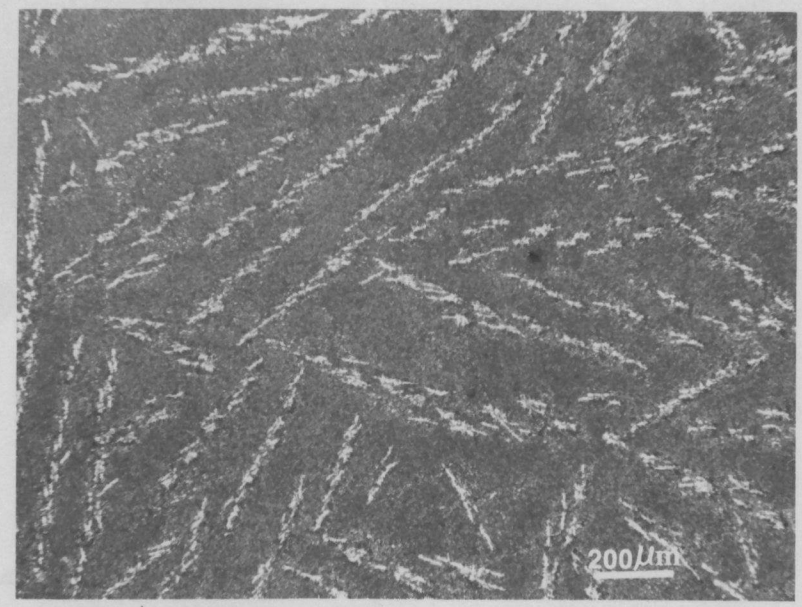
G/R effects. Although directional solidification of the ingots is a steady state and not an equilibrium process, the resulting structures can be interpreted with the use of the phase diagram because equilibrium exists on a local scale at the solid-liquid interface. The equilibrium path of solidification of an alloy is fixed by the equilibrium or tie relationships between the phases, but the steady state path of solidification can change with a change in the growth conditions. The composition of the ingot, the thermal gradient, G and the growth velocity, R, are the important variables to be considered. For the one, two and three phase systems, the G/R ratio is the most convenient and meaningful way to describe the growth conditions (Equations 1 and 7) for the ingot.

For the ingot compositions at the published In-Sn-Cd-Zn eutectic (Ingots 1066, 1070, 1072 and 1088), the steady state path of solidification was changed with changing growth conditions. The ingots were coupled for G/R values between 1.2×10^5 and 1.5×10^5 C-sec/cm^2 and greater than 9×10^5 C-sec/cm^2. The three phase In-Sn-Cd dendrites were observed in the specimens with all other G/R values. This effect is shown in Figure 22.

As the growth conditions approached the conditions where coupled growth occurs, the three phase In-Sn-Cd dendrites decreased

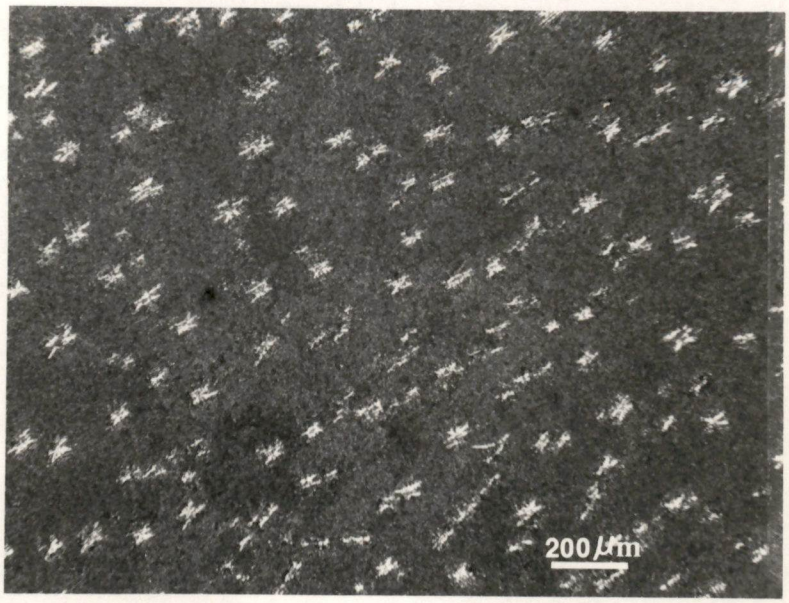


(a) Coupled In-Sn-Cd-Zn, Ingot 1070, G/R = 9.54 x 10^5 C-sec/cm^2.

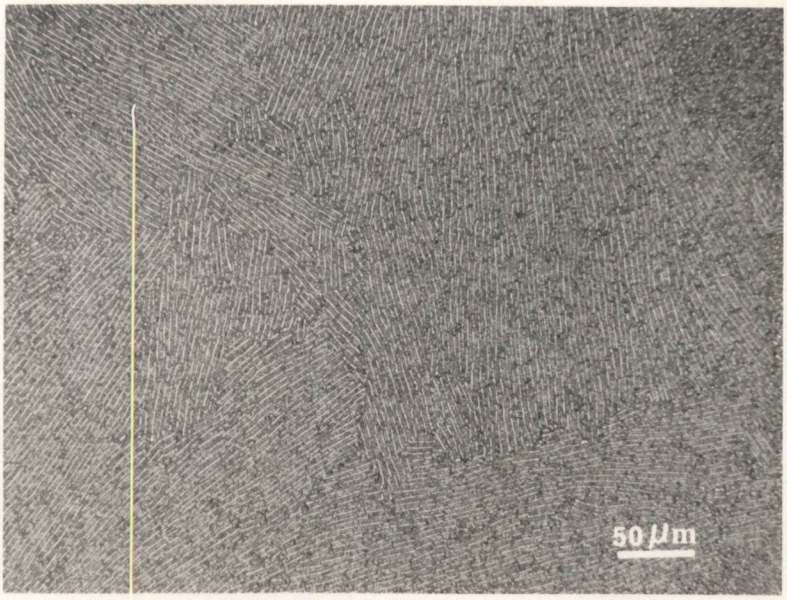


(b) In-Sn-Cd dendrites in In-Sn-Cd-Zn matrix, Ingot 1088, G/R = 1.88 x 10^5 C-sec/cm^2.

Figure 22. Effect of growth conditions on the steady state solidification path.

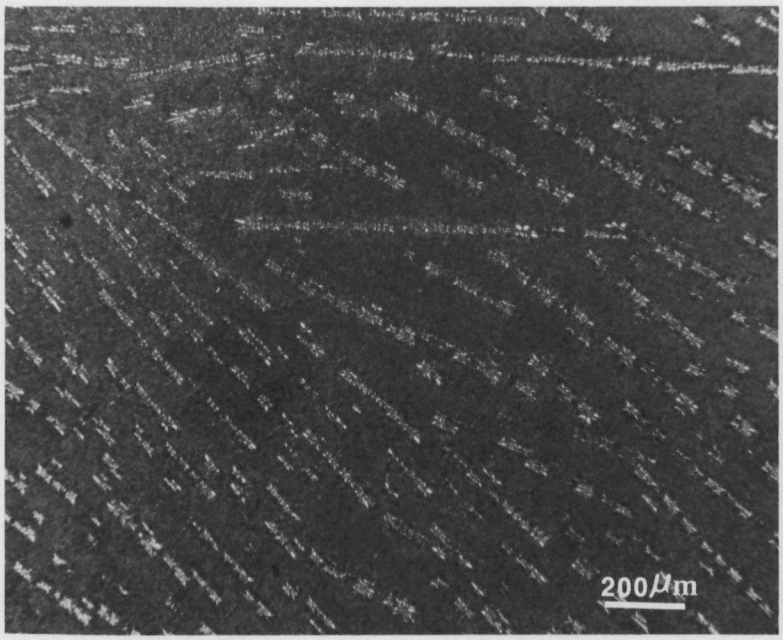


(c) In-Sn-Cd dendrites in In-Sn-Cd-Zn matrix, Ingot 1088, G/R = 1.40 x 10^5 C-sec/cm^2.



(d) Coupled In-Sn-Cd-Zn, Ingot 1066, G/R = 1.20 x 10^5 C-sec/cm^2.

Figure 22. (continued)



(e) In-Sn-Cd dendrites in In-Sn-Cd-Zn matrix, Ingot 1070, G/R = 1.05 x 10^5 C-sec/cm^2.

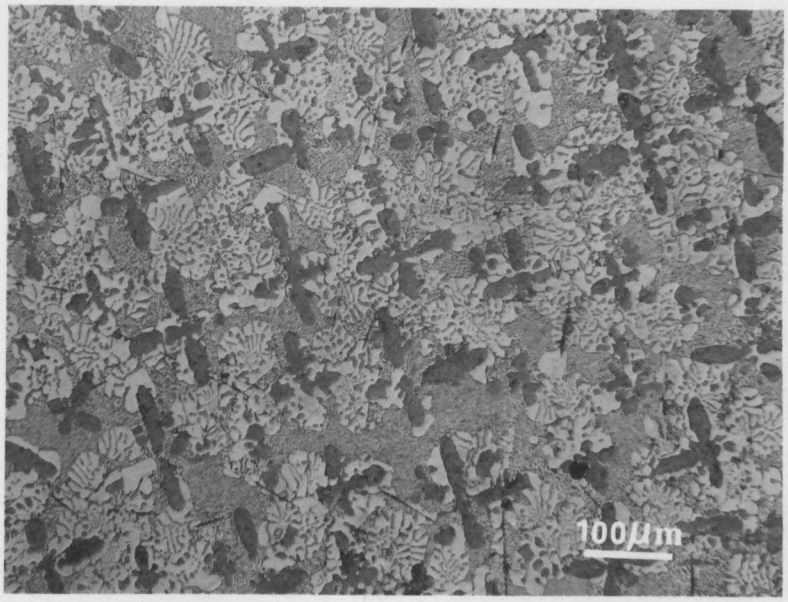
Figure 22. (continued)

in size and in density. This effect is similar to that reported by Holder and Oliver[7] for single phase dendrites in the Pb-Sn-Cd ternary sytem.

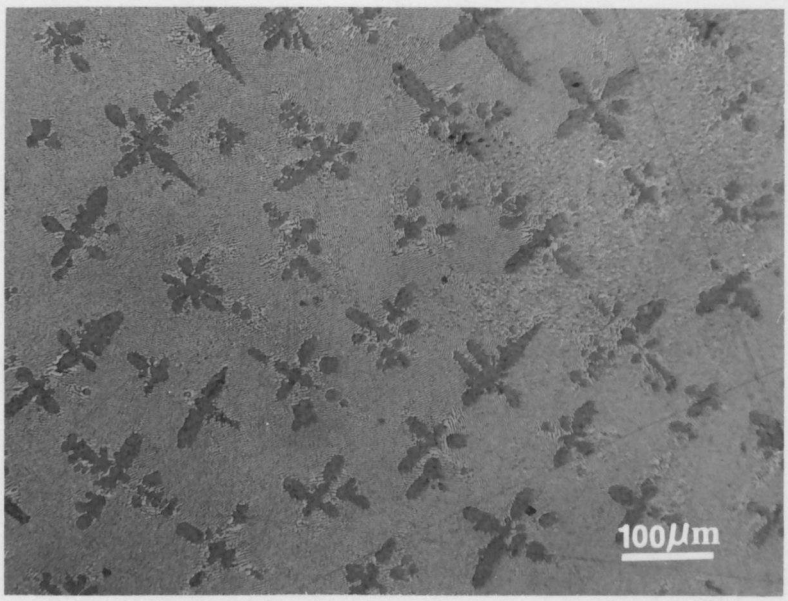
Holder and Oliver also reported a case where the structure of a ternary Pb-Sn-Cd ingot changed from a mixture of one and two phase dendrites to one where only single phase dendrites were present when the growth conditions were changed. A similar effect was observed in all of the off-eutectic ingots in the Pb-Sn-Cd-Zn system. In general, the multiphase dendrites disappeared as the G/R values were increased. With a further increase in G/R, both the Pb and Sn rich ingots, Ingots 1102 and 1098, respectively, became coupled. This is shown in Figure 23 for Ingot 1102. This indicates that as the growth conditons approaches the conditions where coupled growth occurs, the solidification path of the ingot shifts such that the multiphase dendrites disappear first, followed by the primary single phase dendrites. The results also implies that there must exist some critical G/R value for the transitions of the dendritic structures. There is at present no known theory that addresses the problem of the "stability" of dendritic structures to account for the observed transitions in the dendrite structures.

Velocity Effects

Increasing the growth velocity had the same general effect on all the dendrites. The dendrite branching was found to increase and the denrites became finer and more uniformly and densely distributed in the specimen as the growth velocity was increased. The effect of the growth velocity on the Cd-Sn dendrites in Ingot 1076 is

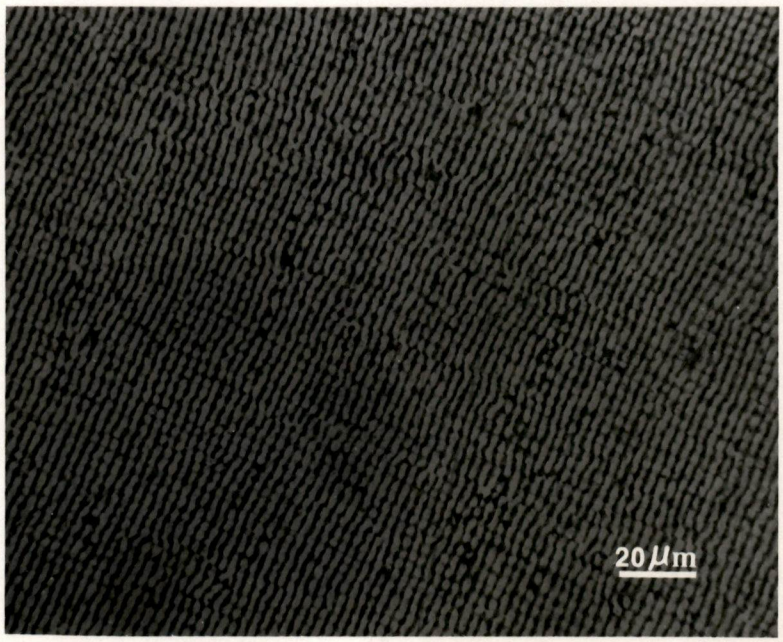


(a) Pb, Pb-Sn and Pb-Sn-Cd dendrites in Pb-Sn-Cd-Zn matrix, G/R = 3.32 x 10^5 C-sec/cm^2.



(b) Pb dendrites in Pb-Sn-Cd-Zn matrix, G/R = 6.43 x 10^5 C-sec/cm^2.

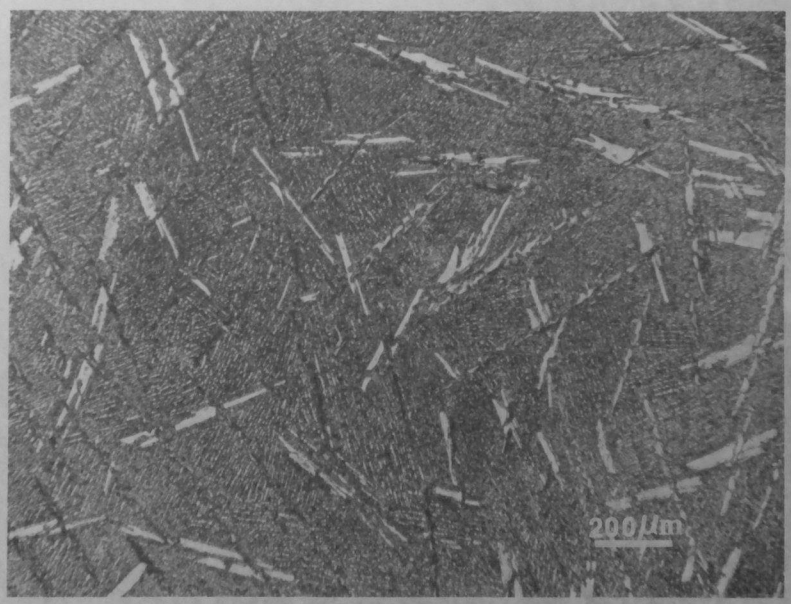
Figure 23. Variation in dendrite structure with growth conditions in Ingot 1102.



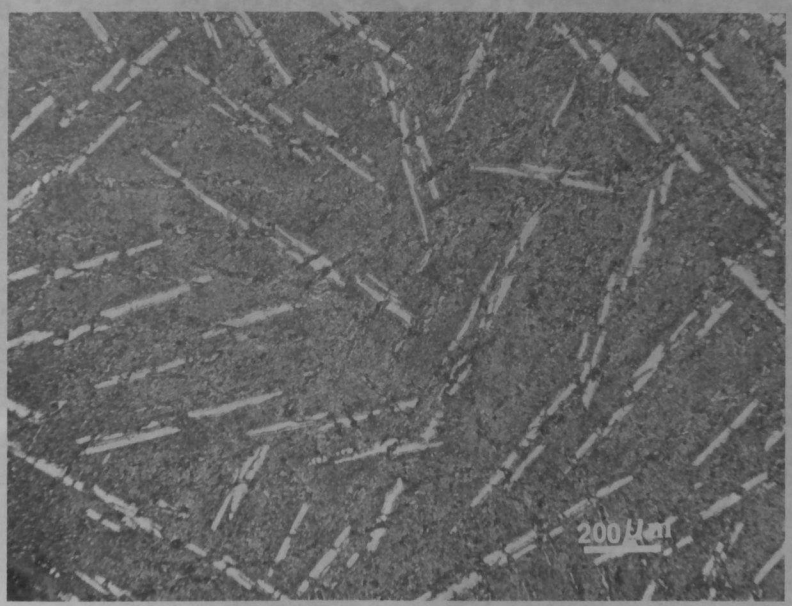
(c) Coupled Pb-Sn-Cd-Zn, G/R = 10.6 x 10^5 C-sec/cm^2.

Figure 23. (continued)

illustrated in Figure 24. The only cases where the dendrite density decreased with increasing growth velocity were in the ingots at the published In-Sn-Cd-Zn eutectic composition (Figure 23). The growth conditions of the specimen placed it in the transition region between the two different steady state solidification paths and is the cause of the observed behavior.

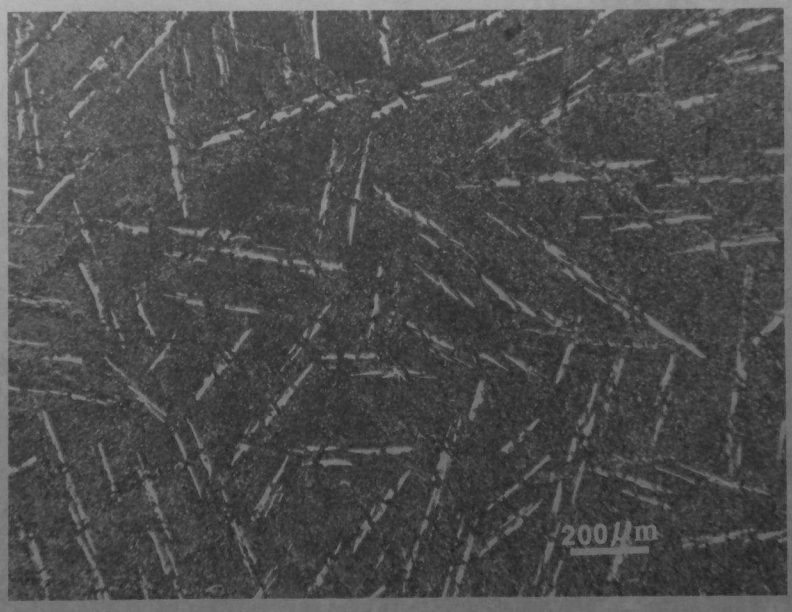


(a) R = 2.54 x 10^{-4} cm/sec.

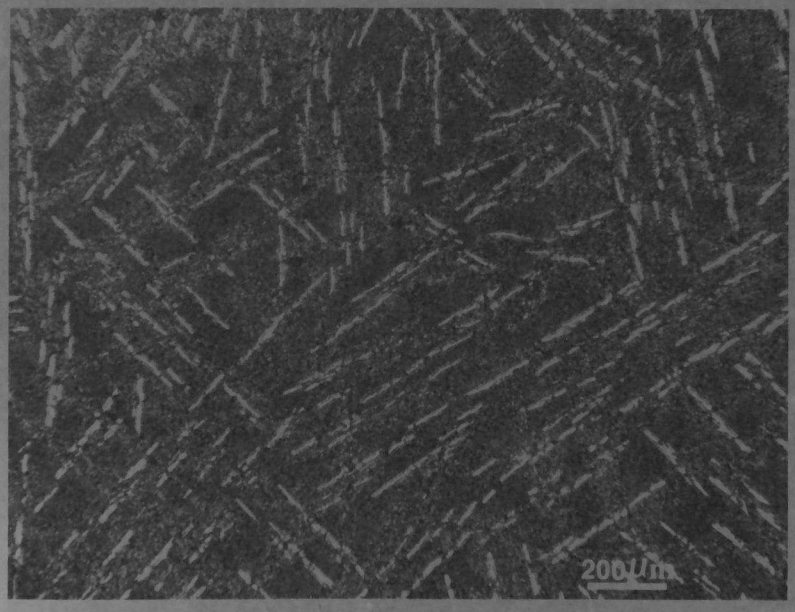


(b) R = 6.16 x 10^{-4} cm/sec.

Figure 24. Effect of growth velocity on the Cd-Sn dendrites in Ingot 1076.



(c) R = 10.7 x 10^{-4} cm/sec.



(d) R = 19.0 x 10^{-4} cm/sec.

Figure 24. (continued)

CHAPTER IV

CONCLUSIONS

1 Coupled four phase growth is possible and was achieved in the two quaternaries studied. For the G/R values examined, the volume of compositions where coupled growth occurs in the Pb-Sn-Cd-Zn system lies within 5 wt% of the eutectic composition and widens out towards the Pb and Sn rich compositions as the G/R value increases. The volume of compositions where coupled growth occurs in the In-Sn-Cd-Zn system is bounded within 5 wt% of the eutectic composition in the Sn, Cd and Zn rich directions but opens up in the In rich direction. The extent of this volume was not determined.

2 Both quaternary eutectics studied contain only very small amounts of Zn. The coupled four phase structures are not significantly different from the coupled structures of the ternaries of the three major volume fraction phases.

3 The quaternaries obey the $\lambda^2 R$ extremum condition for coupled growth. The lamellar spacings of these quaternaries are identical to the lamellar spacings of the ternaries of the three highest volume phases.

It is apparent that the addition of Zn to both the Pb-Sn-Cd and the In-Sn-Cd ternaries to form the two quaternaries does not affect the basic ternary morphology due to the small amount of Zn present. It would be of interest to identify a quaternary whose eutectic contains at least 10-15 % of each of the four phases in order to fully

determine the effect of the addition of the fourth phase on the microstructures in relation to the other variables that affect the morphologies of the ternaries.

4 The interdendritic eutectic in the quaternaries obeys the same $\lambda^2 R$ extremum condition as the coupled eutectics.

5 The temperature profile at the solid-liquid interface is a useful indicator of the microstructures of the specimens. When a single, sharp thermal break at the eutectic is observed, a coupled structure is found. The specimen is dendritic when the thermal break is rounded or when two thermal breaks are seen. The higher temperature of the two thermal breaks corresponds to the liquidus temperature of the alloy.

The temperature at which the thermal breaks occurred in the In-Sn-Cd-Zn ingots provided the evidence for the existence of a coupled four phase structure even though the Zn phase was too small to be directly observed.

6 The measured lamellar spacings of the Pb-Sn-Cd-Zn eutectic agrees with Holder and Oliver's results for the ternary Pb-Sn-Cd eutectic but differs from that reported by Fisher and Kurz for the quaternary and Bao and Durand for the ternary. The results of the last two works agree with each other. It was determined that that gradient used did not significantly affect the lamellar spacings, and that the differences were most probably due to differences in experimental procedures and equipments.

7 The types of dendrites found in the ingots are consistent with the primary phase fields of the phase constitution diagrams.

The path of solidification of the ingots could be inferred from the types of dendrites that were present.

The leading phase in the off-eutectic composition ingots is the primary phase. The primary dendrites extend into the liquid ahead of the eutectic interface until the tips of the dendrites are at the liquidus temperature. The extension of the dendrites ahead of the eutectic can be calculated in the ingots where two thermal breaks are observed.

8 The steady state path of solidification of the alloys can change with a change in the growth conditions. The changing path of solidification with growth condition is evidenced by variations in the types of dendrites in the ingots. The transitions in the dendrite structures indicate the existence of a dendrite "stability" problem for which there exists no theory to account for the observed changes.

9 As the growth velocity increases, the dendrite branching increases and the dendrites become finer and more uniformly and densely distributed in the specimens.

LIST OF REFERENCES

LIST OF REFERENCES

1. W. G. Pfann, *Principles of Zone Melting*, Monogram 2000, Bell Telephone Systems Technical Publications, 1952.

2. J. W. Rutter and B. Chalmers, *Can. J. Phys.*, 1953, vol 31, p 15.

3. W. A. Tiller, K. A. Jackson, J. W. Rutter and B. Chalmers, *Acta Met.*, 1953, vol 1, p 428.

4. W. W. Mullins and R. F. Sekerka, *J. Appl. Phys.*, 1964, vol 35, p 444.

5. W. A. Tiller, "Polyphase Solidification", *Liquid Metals and Solidification*, American Society for Metals, 1958, p 276.

6. H. W. Kerr, A. Plumtree and W. C. Winegard, *J. Inst. Met.*, 1964, vol 93, p 63.

7. J. D. Holder and B. F. Oliver, *Met. Trans.*, 1974, vol 5, p 2423.

8. O. Kubachewski, E. Evans and C. A. Alcock, *Metallurgical Thermochemistry, 4th Edition*, Pergammon Press, New York, 1967.

9. J. H. Holloman and D. Turnbull, *Progress in Metal Physics*, 1953, vol 4, p 333.

10. M. J. Stowell, *Phil. Mag.*, 1970, vol 22, p 1.

11. B. Mustaftschiev and J. Zell, *Surface Science*, 1968, vol 12, p 317.

12. N. Eustathopoulos, J. Joud and P. Desré, *J. de Chimie Physique*, 1974, vol 71, p 777.

13. G. A. Chadwick, *J. Inst. Met.*, 1963/64, vol 92, p 18.

14. E. P. Whelan and C. Haworth, *J. Inst. Met.*, 1964/65, vol 93, p 402.

15. A. Moore and R. Elliot, *J. Inst. Met.*, 1967, vol 95, p 369.

16. B. L. Jones, *J. Aust. Inst. Met.*, 1969, vol 14, p 111.

17. H. O. K. Kirchner and G. A. Chadwick, *J. Cryst. Growth*, 1971, vol 8, p 252.

18. A. Moore and R. Elliot, "Interface Undercooling During Eutectic Solidification", *The Solidification of Metals*, ISI Publication 110, London, 1967, p 167.

19. E. P. Whelan and C. Haworth, *J. Aust. Inst. Met.*, 1967, vol 12, p 77.

20. J. D. Hunt and K. A. Jackson, *Trans TMS-AIME* , 1967, vol 239, p 1129.

21. Ha-Quac Bao, PhD Dissertation, *Universite de Grenoble*, October, 1970.

22. H. E. Cline, *Trans. TMS-AIME*, 1968, vol 242, p 1613.

23. M. D. Rinaldi, R. M. Sharp and M. C. Flemings, *Met. Trans.*, 1972, vol 3, p 3133.

24. D. J. Fisher and W. Kurz, *Met. Trans.*, 1974, vol 5, p 1508.

25. A. Stoffel, *Z. Anorg. Chem.*, 1907, vol 53, p 159.

26. E. Gebhardt, *Z. Metall.*, 1949, vol 40, p 437.

27. E. Lindner, *Z. Metall.*, 1951, vol 42, p 377.

28. N. Parravano and G. Sirovich, *Gazz. Chim. Ital.*, 1912, vol 42, p 630.

29. H. Spengler, *Metallwiss Tech.*, 1960, vol 14, p 789.

30. H. Spengler, *Metall*, 1954, vol 8, p 936.

31. D. J. S. Cooksey and A. Hellawell, *J. Inst. Met.*, 1967, vol 95, p 183.

32. H. W. Kerr, J. A. Bell and W. C. Winegard, *J. Aust. Inst. Met.*, 1965, vol 10, p 64.

33. M. Hansen, *Constitution of Binary Alloys*, McGraw Hill, New York, 1958.

APPENDIX

Table IV lists all the compositions of the ingots studied in the Pb-Sn-Cd-Zn quaternary system. Table V lists all the compositions studied in the In-Sn-Cd-Zn quaternary system. Complete information on the growth conditions (thermal gradient, growth velocity and thermal breaks) is given. The microstructure for each specimen is also listed.

TABLE IV

Pb-Sn-Cd-Zn EXPERIMENTAL RESULTS

Ingot Number	Alloy Composition (%Pb)	(%Sn)	(%Cd)	(%Zn)	Thermal Break(s) (C)	G (C/cm)	R (cm/sec) x10^{4}	G/R (C-sec/cm^{2}) x10^{-5}	Morphology[a]
1092[b]	32.0	49.0	19.0	-----	145	81.1	2.64	3.07	CL
							3.69	2.20	CL
							6.64	1.22	CL
							9.34	0.869	CL
							12.5	0.649	CL
							16.7	0.484	CL
							20.9	0.389	CL
							25.4	0.319	CL
							32.3	0.251	CL
							36.0	0.225	CL
							40.5	0.200	CL
1094[b]	32.0	49.0	19.0	-----	145	386	2.35	16.5	CL
							3.28	11.8	CL
							6.08	6.34	CL
							9.19	4.20	CL
							12.3	3.15	CL
							16.1	2.40	CL
							23.8	1.62	CL
							35.3	1.09	CL
1038	28.6	52.4	16.7	2.3	138	256	2.70	9.48	CL
							12.3	2.09	CL
							20.2	1.27	CL

TABLE IV (continued)

Ingot Number	Alloy Composition (%Pb)	(%Sn)	(%Cd)	(%Zn)	Thermal Break(s) (C)	G (C/cm)	R (cm/sec) $x10^{4}$	G/R (C-sec/cm^2) $x10^{-5}$	Morphology[a]
1064	28.6	52.4	16.7	2.3	138	173	1.30	13.3	CL
							4.75	3.64	CL
1090	29.1	53.2	15.4	2.3	138	79.6	2.94	3.26	CL
							3.82	2.08	CL
							6.14	1.30	CL
							9.28	0.858	CL
							12.1	0.657	CL
							16.0	0.496	CL
							20.5	0.387	CL
							26.0	0.306	CL
							31.6	0.252	CL
							35.8	0.222	CL
							40.1	0.198	CL
1096	27.2	49.8	15.8	7.2	145	257	1.99	12.9	D-I (Zn)
					138		3.95	6.50	D-I (Zn)
							6.01	4.28	D-mixed (Zn) (Pb-Sn-Zn)
							8.87	2.89	D-mixed (Zn) (Pb-Sn-Zn)
							12.1	2.11	D-mixed (Zn) (Pb-Sn-Zn)
							15.6	1.65	D-mixed (Zn) (Pb-Sn-Zn)
							20.0	1.17	D-mixed (Zn) (Pb-Sn-Zn)
							30.4	0.847	D-I (Zn)
							39.7	0.648	D-mixed (Zn) (Pb-Sn-Zn)

TABLE IV (continued)

Ingot Number	Alloy Composition (%Pb)	(%Sn)	(%Cd)	(%Zn)	Thermal Break(s) (C)	G (C/cm)	R (cm/sec) $x10^{4}$	G/R (C-sec/cm^2) $x10^{-5}$	Morphology[a]
1098	25.4	57.4	14.9	2.3	145	295	2.54	9.66	CL
					138		3.77	6.49	CL
							6.09	4.03	D-I (Sn)
							8.93	2.47	D-mixed (Sn) (Pb-Sn-Cd)
							12.3	1.99	D-mixed (Sn) (Pb-Sn-Cd)
							16.2	1.51	D-mixed (Sn) (Pb-Sn-Cd)
							20.3	1.21	D-mixed (Sn) (Pb-Sn-Cd)
							30.2	0.810	D-I (Sn)
							39.8	0.615	D-I (Sn)
1100	26.8	49.1	21.8	2.3	150	247	2.47	9.98	D-I (Cd)
					138		3.77	6.54	D-I (Cd)
							6.08	4.06	D-III (Pb-Sn-Cd)
							9.07	2.72	D-III (Pb-Sn-Cd)
							12.4	1.98	D-III (Pb-Sn-Cd)
							16.2	1.53	D-III (Pb-Sn-Cd)
							20.5	1.21	D-III (Pb-Sn-Cd)
							30.7	0.804	D-I (Cd)
							39.4	0.626	D-III (Pb-Sn-Cd)
1102	33.6	48.6	15.5	2.3	147	389	1.99	19.6	D-I (Pb)
					138		3.66	10.6	CL[c]
							6.05	6.43	D-I (Pb)
							8.65	4.50	D-mixed (Pb) (Pb-Sn) (Pb-Sn-Cd)

TABLE IV (continued)

Ingot Number	Alloy Composition (%Pb)	(%Sn)	(%Cd)	(%Zn)	Thermal Break(s) (C)	G (C/cm)	R (cm/sec) x10^4	G/R (C-sec/cm^2) x10^{-5}	Morphology[a]
							11.7	3.32	D-I (Pb)
							15.7	2.48	D-mixed (Pb) (Pb-Sn) (Pb-Sn-Cd)
							20.5	1.89	D-mixed (Pb) (Pb-Sn) (Pb-Sn-Cd)
							30.8	1.26	D-mixed (Pb) (Pb-Sn) (Pb-Sn-Cd)
							39.9	0.947	D-mixed (Pb) (Pb-Sn) (Pb-Sn-Cd)

[a]CL--coupled lamellar structure.
D-X--dendritic, multiphase dendrite, X number of phases in dendrite. Phases are listed in parenthesis.
D-mixed--different types of dendrites present. Phases are listed in parenthesis.

[b]Ingots 1092 and 1094 were drawn from the same melt.

TABLE V

In-Sn-Cd-Zn EXPERIMENTAL RESULTS

Ingot Number	Alloy Composition (%In)	(%Sn)	(%Cd)	(%Zn)	Thermal Break(s) (C)	G (C/cm)	R (cm/sec) x10^4	G/R (C-sec/cm^2) x10^{-5}	Morphology[a]
1050	44.0	42.0	14.0	-----	93	213	4.55	4.68	D-I (Cd)
							14.7	1.45	D-mixed (Cd) (Sn-Cd)
1052[b]	45.0	43.0	12.0	-----	92.5	220	6.00	3.67	CL
							18.3	1.20	D-I (Sn)
1056[b]	45.0	43.0	12.0	-----	92	184	3.48	5.29	CL
							12.8	1.44	D-I (Sn)
1084	49.0	38.2	12.8	-----	94	205	2.43	8.39	CL
							4.60	4.44	CL
							9.10	2.24	CL
							12.9	1.58	CL
							16.2	1.26	CL
							20.7	0.986	CL
1066[c]	44.2	41.4	13.6	0.8	86.5	196	4.61	4.25	D-I (Sn)
							16.4	1.20	CL
1070[c]	44.2	41.4	13.6	0.8	85	206	2.16	9.54	CL
							8.98	2.29	D-III (In-Sn-Cd)
							12.1	1.70	D-III (In-Sn-Cd)
							19.7	1.05	D-III (In-Sn-Cd)

TABLE V (continued)

Ingot Number	Alloy Composition (%In)	(%Sn)	(%Cd)	(%Zn)	Thermal Break(s) (C)	G (C/cm)	R (cm/sec) x10^4	G/R (C-sec/cm^2) x10^{-5}	Morphology[a]
1072	44.2	41.4	13.6	0.8	84.5	227	2.47	9.15	CL
							8.07	2.81	D-III (In-Sn-Cd)
							15.2	1.49	CL
1088	45.4	40.2	13.6	0.8	86	223	2.48	8.99	D-III (In-Sn-Cd)
							6.09	3.69	D-III (In-Sn-Cd)
							8.40	2.66	D-III (In-Sn-Cd)
							9.06	2.47	D-III (In-Sn-Cd)
							11.9	1.88	D-III (In-Sn-Cd)
							15.7	1.42	D-III (In-Sn-Cd)
							20.2	1.11	D-III (In-Sn-Cd)
							39.4	0.567	D-III (In-Sn-Cd)
1074	41.9	39.2	12.9	6.0	86	205	2.37	8.65	D-mixed (Zn) (Zn-In) (In-Sn-Cd)
							3.81	5.38	D-mixed (Zn) (Zn-In) (In-Sn-Cd)
							6.02	3.41	D-mixed (Zn) (Zn-In) (In-Sn-Cd)
							8.30	2.47	D-mixed (Zn) (Zn-In) (In-Sn-Cd)
							10.6	1.93	D-mixed (Zn) (Zn-In) (In-Sn-Cd)
							14.8	1.38	D-mixed (Zn) (Zn-In) (In-Sn-Cd)
							19.3	1.06	D-mixed (Zn) (Zn-In) (In-Sn-Cd)

TABLE V (continued)

Ingot Number	Alloy Composition (%In)	(%Sn)	(%Cd)	(%Zn)	Thermal Break(s) (C)	G (C/cm)	R (cm/sec) x10^4	G/R (C-sec/cm^2) x10^{-5}	Morphology[a]
1076	41.8	39.3	18.1	0.8	119.5	221	2.54	8.70	D-II (Cd-Sn)
					88		4.18	5.29	D-II (Cd-Sn)
							6.16	3.59	D-II (Cd-Sn)
							8.26	2.68	D-II (Cd-Sn)
							10.7	2.06	D-II (Cd-Sn)
							15.3	1.45	D-II (Cd-Sn)
							18.9	1.17	D-II (Cd-Sn)
1078	49.2	37.6	12.4	0.8	85	208	2.41	8.63	CL
							3.78	5.50	CL
							4.84	4.30	CL
							6.76	3.09	CL
							9.42	2.21	CL
							12.5	1.66	CL
							16.3	1.28	CL
							20.5	1.01	CL
1080	40.4	46.4	12.4	0.8	104	235	1.61	14.6	D-mixed (Sn) (Sn-Cd) (In-Sn-Cd)
					85		3.05	7.70	D-mixed (Sn) (Sn-Cd) (In-Sn-Cd)
							4.03	5.83	D-mixed (Sn) (Sn-Cd) (In-Sn-Cd)
							6.05	3.88	D-mixed (Sn) (Sn-Cd) (In-Sn-Cd)
							8.23	2.86	D-mixed (Sn) (Sn-Cd) (In-Sn-Cd)

TABLE V (continued)

Ingot Number	Alloy Composition (%In)	(%Sn)	(%Cd)	(%Zn)	Thermal Break(s) (C)	G (C/cm)	R (cm/sec) $x10^{4}$	G/R (C-sec/cm^2) $x10^{-5}$	Morphology[a]
							11.7	2.01	D-mixed (Sn) (Sn-Cd) (In-Sn-Cd)
							16.2	1.45	D-mixed (Sn) (Sn-Cd) (In-Sn-Cd)
							19.3	1.22	D-mixed (Sn) (Sn-Cd) (In-Sn-Cd)

[a]CL--coupled lamellar structure.
D-X--dendritic, multiphase dendrite, X number of phases in dendrite. Phases are listed in parenthesis.
D-mixed--different types of dendrites present. Phases are listed in parenthesis.

[b]Ingots 1052 and 1056 were drawn from the same melt.

[c]Ingots 1066 and 1070 were drawn from the same melt.

VITA

Warren Tan King was born in Manila, Philippines on June 12, 1955. He attended elementary and high school at Xavier School, a Jesuit run educational facility just outside Manila.

In April, 1972 his family immigrated to the United States. He entered the University of Tennessee where he obtained both his B.S. and M.S. degrees in Metallurgical Engineering.